Impact of Centre Vortices on the Gluon Propagator

THE UNIVERSITY of ADELAIDE

James Biddle

Supervisors: Prof. Derek B. Leinweber
Dr. Waseem Kamleh

Department of Physics
University of Adelaide

This dissertation is submitted for the degree of
Master of Philosophy
November 2018

Table of contents

I would like to dedicate this thesis to

Declaration

I certify that this work contains no material which has been accepted for the award of any other degree or diploma in my name, in any university or other tertiary institution and, to the best of my knowledge and belief, contains no material previously published or written by another person, except where due reference has been made in the text. In addition, I certify that no part of this work will, in the future, be used in a submission in my name, for any other degree or diploma in any university or other tertiary institution without the prior approval of the University of Adelaide and where applicable, any partner institution responsible for the joint-award of this degree.

I give permission for the digital version of my thesis to be made available on the web, via the University's digital research repository, the Library Search and also through web search engines, unless permission has been granted by the University to restrict access for a period of time.

I acknowledge the support I have received for my research through the provision of an Australian Government Research Training Program Scholarship.

James Biddle
November 2018

Acknowledgements

And I would like to acknowledge ...

Abstract

This is where you write your abstract ...

List of figures

List of tables

Chapter 1

Introduction

Chapter 2

Lattice QCD

Since the first efforts to construct a non-perturbative approach to QCD in 1974[1], lattice QCD has developed over the past 40 years into a powerful tool used to probe the low-energy behaviour of the strong nuclear force. Rather than treat spacetime as a set of continuous axes, it is instead discretised into a finite set of points on a four-dimensional hypercube. This prescription allows for the explicit calculation of path integrals present in QCD, at the cost of introducing finite-spacing errors that must be systematically accounted for. In this chapter we will discuss the behaviour of QCD when spacetime is continuous (hereafter referred to as the continuum), and demonstrate how the transition can be made to a finite set of coordinates on a lattice. We will also describe the two choices of gauge used in this research, and how they are applied to the lattice.

2.1 QCD in the Continuum

2.1.1 Quarks and Gauge Invariance

QCD is the gauge field theory that describes the interactions of quarks and gluons. Like all gauge theories, it has an internal symmetry group which the Lagrangian is invariant under. In the case of QCD there are three quark colours, which leads to the symmetry group being $SU(3)$, the group of 3×3 unitary matrices of determinant 1 [1]. We can see this $SU(3)$ symmetry by inspecting the QCD quark Lagrangian

$$\mathcal{L} = \bar{\psi}(x)\left(i\not{\partial} - m\right)\psi(x)\,. \tag{2.1}$$

[1]This description is only true in the fundamental representation of the group, but this is the symmetry we observe in the Lagrangian and is a useful way to visualise the group symmetry.

If we apply an $SU(3)$ transformation Ω to the colour indices of the quark, $\psi(x)$, and anti-quark, $\bar{\psi}(x)$, fields, we see that

$$\begin{aligned}\mathcal{L} \to \mathcal{L}' &= \bar{\psi}(x)\,\Omega^\dagger\,(i\partial\!\!\!/ - m)\,\Omega\,\psi(x) \\ &= \bar{\psi}(x)\,(i\partial\!\!\!/ - m)\,\psi(x)\,\Omega^\dagger\,\Omega \\ &= \bar{\psi}(x)\,(i\partial\!\!\!/ - m)\,\psi(x) \\ &= \mathcal{L}\,.\end{aligned}$$

Here we have made use of the unitarity property $U\,U^\dagger = I$. If this symmetry were all we required then we would be done and our theory would be pleasantly simple. However, we find that we need our gauge symmetry to be *local*; that is, we demand that our gauge transformation itself be a function of x[2]. In this case, we find that the derivative in Eq. 2.1 results in a loss of $SU(3)$ symmetry. We can write an arbitrary $SU(3)$ gauge transformation as an exponential of the traceless, Hermitian group generators λ_a (known as the Gell-Mann matrices) such that $\Omega = \exp\left(i\omega^a(x)\,\frac{\lambda_a}{2}\right)$. Using this form for Ω, we find that under a gauge transformation the Lagrangian is now

$$\begin{aligned}\mathcal{L} \to \mathcal{L}' &= \bar{\psi}(x)\,\Omega^\dagger(x)\,(i\partial\!\!\!/ - m)\,\Omega(x)\,\psi(x) \\ &= \bar{\psi}\,\Omega^\dagger\left[-\frac{\lambda_a}{2}\,(\partial\!\!\!/\,\omega^a(x)) + i\,\Omega\,(\partial\!\!\!/\,\psi) - m\,\Omega\,\psi\right] \\ &= \mathcal{L} - \bar{\psi}\,\Omega^\dagger\,\frac{\lambda_a}{2}(\partial\!\!\!/\,\omega^a(x))\,\Omega\,\psi \qquad (2.2)\end{aligned}$$

To amend this, we introduce the notion of the gauge-covariant derivative

$$D_\mu = \partial_\mu - igA_\mu(x)\,, \qquad (2.3)$$

where $A_\mu(x) = A^a_\mu(x)\,\frac{\lambda_a}{2}$, and $A^a_\mu(x)$ are eight new 'gauge potentials'. Making the substitution $\partial_\mu \to D_\mu$, we introduce a new term into the Lagrangian that gives rise to an interaction between our quark and gauge fields.

$$\mathcal{L}_{\text{int}} = g\,\bar{\psi}\,A_\mu(x)\,\psi \qquad (2.4)$$

To preserve the gauge invariance of the Lagrangian, we need the gauge transformation property of Eq. 2.4 to counteract the last term of Eq. 2.2. Hence we require that

$$g\,\bar{\psi}\,A_\mu(x)\,\psi \to g\,\bar{\psi}\,A_\mu(x)\,\psi + \bar{\psi}\,\Omega^\dagger\,\frac{\lambda_a}{2}(\partial_\mu\,\omega^a(x))\,\Omega\,\psi\,. \tag{2.5}$$

Making use of the transformation properties of ψ and $\bar{\psi}$, this implies that

$$A_\mu(x) \to \Omega\,A_\mu(x)\,\Omega^\dagger - \frac{i}{g}\,(\partial_\mu\,\Omega)\,\Omega^\dagger\,. \tag{2.6}$$

This transformation property can also be expressed in terms of the covariant derivative. Doing so, we find that

$$\begin{aligned} D_\mu\,\psi \to &\left(\partial_\mu - ig\,\Omega\,A_\mu(x)\,\Omega^\dagger - (\partial_\mu\,\Omega)\,\Omega^\dagger\right)\,\Omega\,\psi \\ &= (\partial_\mu\,\Omega)\,\psi + \Omega\,(\partial_\mu\,\psi) - ig\,\Omega\,A_\mu(x)\,\psi - (\partial_\mu\,\Omega)\psi \\ &= \Omega\,D_\mu\,\psi\,. \end{aligned}$$

And therefore

$$D_\mu \to \Omega\,D_\mu\Omega^\dagger \tag{2.7}$$

This result tells us that the covariant derivative of a quark field transforms in the same way as the quark field itself. The covariant derivative can then be thought of as a connection between two points that may have a different underlying gauge. For example, if we consider an infinitesimal translation in the quark field

$$d\psi(x) = \psi(x + dx) - \psi(x)\,,$$

we note that the gauge at the point x and at $x + dx$ in general will differ, so it doesn't make sense to compare the field values through the usual understanding of the derivative. Instead, the covariant derivative accounts for this underlying gauge structure, 'transporting' the field from one position to another.

2.1.2 Gluon Field

Using local gauge invariance as a guide, we can now seek other gauge invariant terms to insert into the Lagrangian. If we consider the commutator of the covariant derivative,

we have

$$\begin{aligned}[D_\mu,\, D_\nu] \rightarrow &[\Omega\, D_\mu\, \Omega^\dagger,\, \Omega\, D_\nu\, \Omega^\dagger] \\ &= \Omega\, D_\mu\, D_\nu\, \Omega^\dagger - \Omega\, D_\nu\, D_\mu\, \Omega^\dagger \\ &= \Omega\, [D_\mu,\, D_\nu]\, \Omega^\dagger\,.\end{aligned}$$

We therefore define the gluon field strength tensor to be

$$F_{\mu\nu} = \frac{i}{g}\,[D_\mu,\, D_\nu] \tag{2.8}$$

Expanding this definition, $F_{\mu\nu}$ may also be written

$$F_{\mu\nu} = \partial_\mu A_\nu - \partial_\nu A_\mu - ig[A_\mu,\, A_\nu] \tag{2.9}$$

To obtain a gauge invariant quantity, we take the trace of the contracted field strength tensor. This allows us to make use of the cyclic property of the trace to obtain

$$\begin{aligned}\mathrm{Tr}(F_{\mu\nu}\, F^{\mu\nu}) \rightarrow &-\frac{1}{g^2}\,\mathrm{Tr}\left(\Omega\,[D_\mu,\, D_\nu]\,\Omega^\dagger\,\Omega\,[D^\mu,\, D^\nu]\,\Omega^\dagger\right) \\ &= -\frac{1}{g^2}\,\mathrm{Tr}\left(\Omega^\dagger\,\Omega\,[D_\mu,\, D_\nu]\,[D^\mu,\, D^\nu]\,\right) \\ &= \mathrm{Tr}(F_{\mu\nu}\, F^{\mu\nu})\end{aligned}$$

Thus we define the full gauge invariant QCD Lagrangian to be

$$\mathcal{L}_{\mathrm{QCD}} = \bar{\psi}(x)\,(i\not{D} - m)\,\psi(x) - \frac{1}{2}\,\mathrm{Tr}(F_{\mu\nu}(x)\, F^{\mu\nu}(x)) \tag{2.10}$$

This gluon term is not the only gauge invariant quantity we could construct; for example, $\bar{\psi}\,\psi\,\bar{\psi}\,\psi$ is clearly gauge invariant. However, it turns out that there is a further condition that must be satisfied by each term in the Lagrangian; each term must be *renormalisable*[2]. A complete discussion of renormalisation is unnecessary for this work, but renormalisability can be quickly summarised by looking at the dimensionality of each term in the Lagrangian. The Lagrangian must have units of (Energy)^4, which in natural units is (mass)^4 (hereafter referred to as just dimension 4). We therefore require that each term and its accompanying coupling constant give the same dimensionality. The fermion field has dimension $\frac{3}{2}$, the gauge potential has

dimension 1 and ∂_μ has dimension 1. Then we see that the terms present in Eq. 2.10 have dimension

$$\begin{aligned}
\mathrm{D}[\bar{\psi}(x)\,\gamma^\mu\,\partial_\mu\,\psi(x)] &= \frac{3}{2}+1+\frac{3}{2}=4\\
\mathrm{D}[\bar{\psi}(x)\,\gamma^\mu\,A_\mu\,\psi(x)] &= \frac{3}{2}+1+\frac{3}{2}=4\\
\mathrm{D}[\bar{m\psi}(x)\,\psi(x)] &= 1+\frac{3}{2}+\frac{3}{2}=4\\
\mathrm{D}[F_{\mu\nu}\,F^{\mu\nu}] &= 2+2=4
\end{aligned}$$

as required. This also tells us that the coupling constant g is dimensionless. If a new gauge invariant term $h\bar{\psi}\,\psi\,\bar{\psi}\,\psi$ with coupling constant h is introduced, we then require that h have dimension -2. It turns out that if the dimensionality of the coupling constant is less than 0 then the term in non-renormalisable. This means that integrals involving this new term will diverge in such a way that they cannot be systematically be made finite through use of an ultraviolet cutoff, and hence they cannot form part of any physical theory. By applying the requirements of gauge invariance and renormalisability, it is apparent that Eq. 2.10 is the full QCD Lagrangian.

2.1.3 Pure Gauge Action

For the purpose of this research, we are interested in the behaviour of gluons in the absence of any quarks, and as such we need to develop a description of pure gauge fields. In the continuum, a pure gauge field has the Lagrangian[3]

$$\mathcal{L}_{\text{gluon}} = \frac{1}{2}\,\mathrm{Tr}(F_{\mu\nu}\,F^{\mu\nu})\,, \tag{2.11}$$

which we observe to be the last term in Eq. 2.10. This Lagrangian has the corresponding action

$$\mathcal{S} = \int\, d^4x\;\mathcal{L}_{\text{gluon}}, \tag{2.12}$$

When considering the path integral formulation of a gauge field theory, integrals such as the generating functional,

$$\mathcal{Z} = \int \mathcal{D}A_\mu \exp\left(i\,\mathcal{S}\left[A_\mu(x)\right]\right), \tag{2.13}$$

and others of a similar form appear frequently. This integral closely resembles the partition function found in statistical mechanics, $Z_{\text{classical}} = \int d^3x\,d^3p\,\exp\left(-\beta\,H(x,p)\right)$,

with the notable exception of the factor of i in the exponential. From the statistical mechanics perspective, the exp(...) term in the generating functional is a probability weighting for each 'path' through gauge space. The factor of i in Eq. 2.13 results in an oscillatory weighting, rendering numerical simulations untenable. To ensure that the weight factor is purely real, it is necessary to perform a Wick rotation into Euclidean space[1, 4]

$$x_0 \to -ix_0$$

The generating functional now becomes

$$\mathcal{Z}_{\text{Eucl}} = \int \mathcal{D}A_\mu \exp\left(-\mathcal{S}_{\text{Eucl}}\left[A_\mu(x)\right]\right). \tag{2.14}$$

The Wick rotation also has the consequence of reducing the metric $g_{\mu\nu}$ to the identity, meaning that there is no longer any differentiation between covariant and contravariant tensors.

2.2 Lattice Discretisation

Within this framework, we can now consider discretising spacetime into a finite lattice with N_s lattice sites in the spacial directions and N_t sites in the time direction. Each lattice site is separated by a spacing a, resulting in a total lattice volume $V = (N_s\, a)^3 \times N_t\, a$. This discretisation is shown in two dimensions in Fig. 2.1. We also must impose periodic boundary conditions, such that $x + (N+1)a\hat{\mu} = x$.

When spacetime is discretised, it becomes necessary to consider derivatives as finite differences and integrals as finite sums.

$$\partial_\mu f(x) \to \frac{f(x + a\hat{\mu}) - f(x)}{a}$$
$$\int d^4x\ f(x) \to a^4 \sum_x f(x)$$

For example, we can construct the lattice form of Eq. 2.9 as

$$F^{\mu\nu}_{\text{Lat}}(x) = \frac{A_\nu(x + a\hat{\mu}) - A_\nu(x)}{a} - \frac{A_\mu(x + a\hat{\nu}) - A_\mu(x)}{a} - ig[A_\mu(x),\, A_\nu(x)]. \tag{2.15}$$

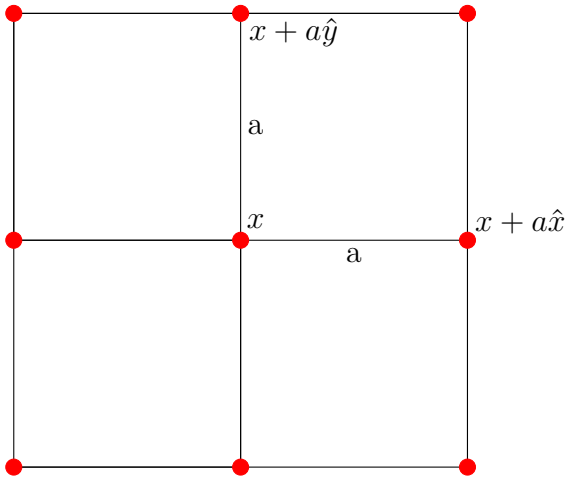

Fig. 2.1 An example of a 2D lattice with lattice spacing a. If we have a position x then we can define $x + a\hat{\mu}$ to represent the next lattice site in the $\hat{\mu}$ direction.

The notation $A_\nu(x + a\hat{\mu})$ denotes the field A_ν located at the site one lattice spacing in the $\hat{\mu}$ direction from x. We could continue to reformulate our lattice theory by imposing this method of discretisation, and indeed this is historically how the lattice framework was constructed[1]. However, it is useful to instead formulate our lattice theory in terms of the gauge *links*. Analogous to how we introduced the covariant derivative to compensate for the fact that the quark field at infinitesimally different points in space has a different underlying gauge, we now want to have a mechanism for comparing quark fields at some finite separation. This requires us to solve the parallel transport equation of our gauge field [5]

$$\frac{dx_\mu(t)}{dt} D_\mu U(x_\mu(t)) = 0, \ t \in [0,1]\,, \tag{2.16}$$

where $U(x_\mu(t))$ is an $SU(3)$ element satisfying $U(x_\mu(0)) = I$. Using the explicit parametrisation $x_\mu = y_\mu + a\,t\,\hat{\sigma}$, where y_μ is a fixed position and σ is a fixed direction, we have

$$\begin{aligned}
&a\,\delta^\sigma_\mu\,(\partial_\mu - igA_\mu)\,U(y_\mu + a\,t\,\hat{\sigma}) = 0\\
&a\partial_\sigma\,U(y_\mu + a\,t\,\hat{\sigma}) = iag\,A_\sigma\,U(y_\mu + a\,t\,\hat{\sigma})\\
&\frac{\partial}{\partial t}U(y_\mu + a\,t\,\hat{\sigma}) = ig\,A_\sigma\,U(y_\mu + a\,t\,\hat{\sigma})\,.
\end{aligned}$$

This is precisely the differential equation solved by the path-ordered exponential, so we find for each direction the gauge links

$$U_\mu(x) = \mathcal{P} \exp\left(ig \int_x^{x+a\hat{\mu}} dx' \, A_\mu(x') \right) . \tag{2.17}$$

From this definition we also see that we can write the gauge link in the opposite direction, i.e. from $x + a\hat{\mu}$ to x, as

$$\begin{aligned} \mathcal{P} \exp\left(ig \int_{x+a\hat{\mu}}^{x} dx' \, A_\mu(x') \right) &= \mathcal{P} \exp\left(-ig \int_x^{x+a\hat{\mu}} dx' \, A_\mu(x') \right) \\ &= U_\mu^\dagger(x) \, . \end{aligned}$$

These gauge links have the simple gauge transformation property [6]

$$U_\mu \to \Omega(x) \, U_\mu(x) \, \Omega^\dagger(x + a\hat{\mu}) \, . \tag{2.18}$$

Making use of this gauge transformation property, we can construct gauge invariant Wilson loops by taking the product of the U_μ's around a closed loop. The simplest such loop, the 1×1 square, is called the *plaquette*, and is defined as

$$P_{\mu\nu}(x) = U_\mu(x) \, U_\nu(x + a\hat{\mu}) \, U_\mu^\dagger(x + a\hat{\nu}) \, U_\nu^\dagger(x) \, . \tag{2.19}$$

Taking the trace of this loop we see that by the cyclic property of the trace this is gauge invariant

$$\begin{aligned} \mathrm{Tr}\left(P_{\mu\nu}(x)\right) \to \mathrm{Tr} \Big(& \Omega(x) \, U_\mu(x) \Omega^\dagger(x + a\hat{\mu}) \, \Omega(x + a\hat{\mu}) \, U_\nu(x + a\hat{\mu}) \, \Omega^\dagger(x + a\hat{\mu} + a\hat{\nu}) \\ & \Omega(x + a\hat{\mu} + a\hat{\nu}) \, U_\mu^\dagger(x + a\hat{\nu}) \, \Omega^\dagger(x + a\hat{\nu}) \, \Omega(x + a\hat{\mu}) \, U_\nu^\dagger(x) \, \Omega^\dagger(x) \Big) \\ = \mathrm{Tr}\left(P_{\mu\nu}(x)\right) \, . \end{aligned}$$

We now return to the lattice formulation, making use of the gauge links to define our quantities of interest. Firstly, we approximate our gauge links using a midpoint approximation, such that

$$U_\mu^{\mathrm{lat}}(x) = \exp\left(iag \, A_\mu\left(x + \frac{a}{2}\hat{\mu} \right) \right) . \tag{2.20}$$

From this definition, we can also recover the the midpoint gauge potential [7, 8]

$$A_\mu\left(x+\frac{a}{2}\hat{\mu}\right)=\frac{1}{2iag}\left(U_\mu(x)-U_\mu^\dagger(x)\right)-\frac{1}{6iag}\operatorname{Tr}\left(U_\mu(x)-U_\mu^\dagger(x)\right)I+\mathcal{O}(a^2)\,. \quad (2.21)$$

We then note that we can write $F_{\mu\nu}$ in terms of the plaquette by Taylor expanding Eq. 2.19 to obtain [9]

$$P_{\mu\nu}=I+ia^2g\,F_{\mu\nu}-\frac{a^4g^2}{2}F_{\mu\nu}F^{\mu\nu}+\mathcal{O}(a^6)\,, \quad (2.22)$$

and hence

$$a^4\operatorname{Tr}\left(F_{\mu\nu}F^{\mu\nu}\right)=\frac{2}{g^2}\operatorname{Tr}\left(I-\frac{1}{2}\left(P_{\mu\nu}+P_{\mu\nu}^\dagger\right)\right)\,. \quad (2.23)$$

We have now arrived at a definition of the contracted field strength tensor that can be used to define our lattice action. As we sum over the 6 unique plaquettes, we take into account a factor of 2 to arrive at the definition

$$\mathcal{S}_{\text{lat}}=\beta\sum_x\sum_{\mu<\nu}\frac{1}{3}\operatorname{Tr}\left(I-\frac{1}{2}\left(P_{\mu\nu}+P_{\mu\nu}^\dagger\right)\right)\,, \quad (2.24)$$

where $\beta=\frac{6}{g^2}$ is the lattice coupling constant. To remove higher order errors from the lattice action, it is possible to take into account terms containing larger Wilson loops, following procedure similar to the one outlined above [10–12].

For the purpose of this work, the gauge fields were generated using the $\mathcal{O}(a^2)$-improved Lüscher and Weisz action [13],

$$\begin{aligned}S_1=&\frac{5\beta}{9}\sum_{\mu<\nu}\operatorname{Tr}\left\{1-\frac{1}{2}\left(P_{\mu\nu}+P_{\mu\nu}^\dagger\right)\right\}\\&-\frac{\beta}{36u_0^2}\sum_{\text{rect}}\operatorname{Tr}\left\{1-\frac{1}{2}\left(R_{\mu\nu}+R_{\mu\nu}^\dagger\right)\right\}\,,\end{aligned} \quad (2.25)$$

where

$$u_0=\left(\frac{1}{3}\operatorname{Re}\operatorname{Tr}\langle P_{\mu\nu}\rangle\right)^{\frac{1}{4}}\,. \quad (2.26)$$

and $R_{\mu\nu}$ is the 2×1 rectangle Wilson loop, defined similarly to the plaquette

$$\begin{aligned} R_{\mu\nu}(x) = \; & U_\mu(x)U_\nu(x+\hat{\mu})U_\nu(x+\hat{\nu}+\hat{\mu})U_\mu^\dagger(x+2\hat{\nu}) \\ & \times U_\nu^\dagger(x+\hat{\nu})U_\nu^\dagger(x) + U_\mu(x)U_\mu(x+\hat{\mu}) \\ & \times U_\nu(x+2\hat{\mu})U_\mu^\dagger(x+\hat{\mu}+\hat{\nu})U_\mu^\dagger(x+\hat{\nu})U_\nu^\dagger(x)\,. \end{aligned} \tag{2.27}$$

The presence of the 'tadpole' improvement factor u_0 is necessary to modify the coupling constant such that the action has better agreement with the continuum over small distances [14]. This choice of action

This lattice framework provides the tools necessary to explicitly calculate quantities of interest from a first-principles standpoint. Firstly, the gauge links are generated by monte-carlo methods, using $\exp(-\mathcal{S})$ as a probability weighting for a given configuration. Once these configurations are generated, gauge fixing can be performed (Sec. 2.3.1, 3.3.1), and quantities such as the gluon propagator (Chapter 4) can be obtained.

2.3 Gauge Fixing

The choice of gauge is crucial when performing calculations on the lattice, or more generally in any gauge field theory calculation. There are two choices of gauge relevant to this study: Landau gauge and maximal centre gauge. Maximal centre gauge is best explored in the context of centre vortices, and will therefore be detailed in chapter 3.3.1, however the Landau gauge fixing condition provides a good introduction to the gauge fixing procedure, and as such will be described here.

2.3.1 Landau Gauge

In the continuum, Landau gauge corresponds to imposing the condition

$$\partial_\mu A^\mu = 0\,. \tag{2.28}$$

On the lattice, we can approximate this condition by imposing

$$\Delta(x) = \sum_\mu A_\mu\left(x + \frac{a}{2}\hat{\mu}\right) - A_\mu\left(x - \frac{a}{2}\hat{\mu}\right) = 0\,. \tag{2.29}$$

Here the fact that we have defined the lattice gauge potential to be at the midpoint of the link produces an improved continuum limit when we consider Eq. 2.29 in momentum space [8]. Performing a discrete Fourier transform, we see that

$$\begin{aligned}
\Delta(p) &= \sum_x \Delta(x) e^{-i\,p\cdot x} \\
&= \sum_{x,\,\mu} e^{-i\,p\cdot x} \left(A_\mu \left(x + \frac{a}{2}\hat{\mu} \right) - A_\mu \left(x - \frac{a}{2}\hat{\mu} \right) \right) \\
&= \sum_{x,\,\mu} e^{i\,p\cdot\frac{a}{2}\hat{\mu}}\, e^{-i\,p\cdot\left(x+\frac{a}{2}\hat{\mu}\right)} A_\mu \left(x + \frac{a}{2}\hat{\mu} \right) - e^{-i\,p\cdot\frac{a}{2}\hat{\mu}}\, e^{-i\,p\cdot\left(x-\frac{a}{2}\hat{\mu}\right)} A_\mu \left(x - \frac{a}{2}\hat{\mu} \right) \\
&= \sum_{\mu} \left(e^{i\,p\cdot\frac{a}{2}\hat{\mu}} - e^{-i\,p\cdot\frac{a}{2}\hat{\mu}} \right) A_\mu(p) \\
&= \sum_{\mu} 2i \sin\left(\frac{a}{2} p_\mu \right) A_\mu(p) = 0\,. \qquad (2.30)
\end{aligned}$$

This is to be compared to the momentum space Landau gauge condition that can be obtained from the gauge potential defined on the lattice sites, which has the form [8]

$$\sum_{\mu} \left[(\cos(a\,p_\mu) - 1) - i \sin(a p_\mu) \right] A'_\mu(p) = 0\,. \qquad (2.31)$$

In the limit as $a \to 0$, it can be seen that Eq. 2.30 exhibits $\mathcal{O}(a^2)$ improvement, whereas Eq. 2.31 has only $\mathcal{O}(a)$ improvement.

The Landau Gauge condition is imposed on the Lattice by finding extrema of the functional [15]

$$\mathcal{F} = \frac{4}{3}\mathcal{F}_1 - \frac{1}{12u_0}\mathcal{F}_2\,, \qquad (2.32)$$

where

$$\begin{aligned}
\mathcal{F}_1 &= \sum_{\mu,x} \frac{1}{2} \operatorname{Tr} \left\{ U^G_\mu(x) + U^G_\mu(x)^\dagger \right\} \\
\mathcal{F}_2 &= \sum_{\mu,x} \frac{1}{2} \operatorname{Tr} \left\{ U^G_\mu(x) U^G_\mu(x + a\hat{\mu}) + \text{h.c.} \right\}\,.
\end{aligned}$$

We explicitly write U^G_μ to indicate that we are considering gauge links under as-yet unknown gauge transformation

$$\Omega(x) = \exp\left(i\omega^a(x) \frac{\lambda_a}{2} \right) \qquad (2.33)$$

It becomes apparent why this we seek the extrema of this particular functional when we take the functional derivative with respect to the free parameters of the gauge transformation, $\omega^a(x)$.

$$\frac{\delta\left\{\frac{4}{3}\mathcal{F}_1 - \frac{1}{12u_0}\mathcal{F}_2\right\}}{\delta\omega^a(x)} = ga^2\sum_\mu \mathrm{Tr}\left\{\left[\partial_\mu A_\mu(x) - \frac{4}{360}a^4\partial_\mu^5 A_\mu(x) + \mathcal{O}\left(a^6\right)\right]\frac{\lambda^a}{2}\right\} + \mathcal{O}\left(g^3a^4\right) \tag{2.34}$$

If Eq. 2.34 is at an extrema, then

$$\sum_\mu \partial_\mu A_\mu(x) = \sum_\mu \frac{4}{360}a^4\partial_\mu^5 A_\mu(x) + \mathcal{O}(a^6) + \mathcal{O}(g^3a^4)\,.$$

Hence at order $\mathcal{O}(a^4)$, finding the extrema of Eq. 2.34 is equivalent to satisfying the continuum Landau gauge condition, Eq. 2.28.

2.4 Lattice units

In the previous section, we have explicitly detailed how a variety of lattice quantities are constructed. For clarity, it is useful to remove extraneous constants by utilising so-called 'lattice units'. Transforming to lattice units is done by setting $a = g = 1$, which gives the following transformations

$$\begin{aligned} A_\mu\left(x + \frac{a}{2}\hat{\mu}\right) &\to A_\mu\left(x + \frac{\hat{\mu}}{2}\right) \\ U_\mu(x) &\to \exp\left(iA_\mu\left(x + \frac{\hat{\mu}}{2}\right)\right) \\ P_{\mu\nu}(x) &\to U_\mu(x)\,U_\nu(x+\hat{\mu})\,U_\mu^\dagger(x+\hat{\nu})\,U_\nu^\dagger(x) \end{aligned}$$

Chapter 3

Topology of the Lattice

QCD presents two properties that distinguish it from the other forces of nature: confinement and dynamical chiral symmetry breaking. Both these properties have been experimentally observed, however a unified theoretical understanding of how they arise from the current standard model of QCD is still a subject of interest.

3.1 Confinement

The confinement property of QCD, and the accompanying notion of asymptotic freedom, is one of the defining low-energy features of the theory of the strong interaction. With Gell-mann and Zweig's concurrent proposal of quarks as the elementary constituents of baryons and mesons [16, 17], it is natural to then attempt to observe these new particles in isolation. However, efforts to observe quarks proved impossible. Early experiments testing the behaviour of electron-proton collisions demonstrated that protons scatter elastically, behaving as though they are finite-sized particles recoiling electromagnetically from the incident electron [18]. These experiments indicated no further substructure to the proton, inconsistent with the quark model. As accelerator energies improved, later experiments [19, 20], using electron energies of 7 and 10 GeV found that inelastic scattering effects became dominant, with electrons behaving as though they were scattering off of loosely bound constituent particles. To explain this behaviour, Feynman proposed what is known as the 'parton' model [21], treating the proton as being comprised of non-interacting electrically charged particles in the limit that the incident electron energy tends towards infinity. This is precisely the notion of asymptotic freedom; at large distance scales the partons are tightly bound, whereas at short distances they behave as free particles. It did not take long for the separate theories of quarks and partons to recognised as complementary, and by the early 70's

the quark-parton model of hadrons accurately explained the the experimental results observed in particle colliders.

These experimental and theoretical results led in part to the development of the non-Abelian gauge field theory of QCD, as introduced in Chapter 2. The proof that non-Abelian gauge theories are asymptotically free was discovered in 1973 [22], and experimental evidence of the existence of 3 quark colours through study of the cross section of e^+e^- collisions supports the initial $SU(3)$ colour symmetry anticipated by Gell-Mann and Zweig. At high energies, QCD has consistently explained the behaviour of hadronic matter, and has become the accepted theory of the strong nuclear interaction. However, the question of whether QCD is indeed a confining theory still remains. As confinement is a low-momentum property of QCD, it is apparent that any analytic proof of confinement must take place far from the asymptotic limit. To date, no such analytic proof has been found.

Lattice calculations are currently the only method by which it is possible to investigate low-energy QCD phenomena from first-principles. Calculations of the static potential between two massive quarks, both recent and old [23–26], have shown that the potential rises linearly at sufficiently large separation distances. This behaviour is precisely what is expected of a colour confining theory. Other confinement mechanisms have also been proposed on the lattice, including mechanisms based on the behaviour of the gluon propagator at $q = 0$ [27] and the behaviour of the pion mass and Polyakov loop at light quark masses [28]. All lattice results so far have indicated that QCD is in fact a confining theory at low energy.

There is good evidence that confinement has its roots in the topological properties of the QCD vacuum. It is well understood that the QCD vacuum, unlike the QED vacuum, admits non-trivial instanton solutions: solutions of the vacuum field configurations that are all minima of the classical action, yet are distinguished from one another by a topological quantum number [29]. The presence of instanton solutions was significant in resolving the $U(1)$ anomaly [30], and provides an excellent method of calculating the ground state hadron spectrum [4]. The non-trivial topology of the QCD vacuum, and the success of topological features in resolving QCD anomalies, motivates the search for a topological explanation of confinement. A variety of features have been proposed, including: Abelian monopoles [31, 32], merons [33] and dual superconductors [34, 35].

One of the most promising models in recent years is known as the *Centre Vortex Model*, and it is this model that forms the backbone of this research.

3.2 Centre Vortices

Originally proposed by 't Hooft in 1978 [36, 37], centre vortices are closed two-dimensional surfaces present in four-dimensional Euclidean space. The key property of a centre vortex is that in three dimensions, where the vortices appear as tubes, any Wilson loop (see Sec. 2.2) that encloses a vortex will acquire a centre phase, such that

$$W(C) \to z\, W(C)\,, \tag{3.1}$$

where z is an element of $Z(3)$, the centre of $SU(3)$. The centre of a group is the subgroup that contains all the elements of the group that commute with all other elements. In the case of $SU(3)$ this corresponds to

$$Z(3) = \left\{ \exp\left(\frac{m\pi i}{3}\right) I \mid m = 0, \pm 1 \right\}. \tag{3.2}$$

When considering the value of any given Wilson loop, the centre vortex model suggests that

$$W(C) = \prod_i z_i \times \{\text{short-distance physics}\}\,, \tag{3.3}$$

where the z_i correspond to the phases of the centre vortices intersecting the loop C. A simple visualisation of this idea is shown in Fig. 3.1. It is not immediately apparent why this form of the Wilson loop is related to confinement, however a simple $SU(2)$ calculation motivates the relevance of this model [38]. To understand the significance of this calculation it is worth first deviating slightly to detail the relationship between the Wilson loop and the potential energy between two massive (static) quarks.

Follwing the argument presented in Ref. [39], consider a Wilson loop calculated around a rectangle in the $x - t$ plane with dimensions $R \times T$. As the Wilson loop is gauge invariant, we are free to select a convenient gauge in which to perform the calculation. To this end, we choose the fields to be in axial gauge, such that $A_0(x) = 0 \implies U_0(x) = 1 \,\forall\, x$. So the Wilson loop becomes

$$W(R \times T) = \mathrm{Tr}\left(U_1(0)\, U_1^\dagger(T)\right)\,. \tag{3.4}$$

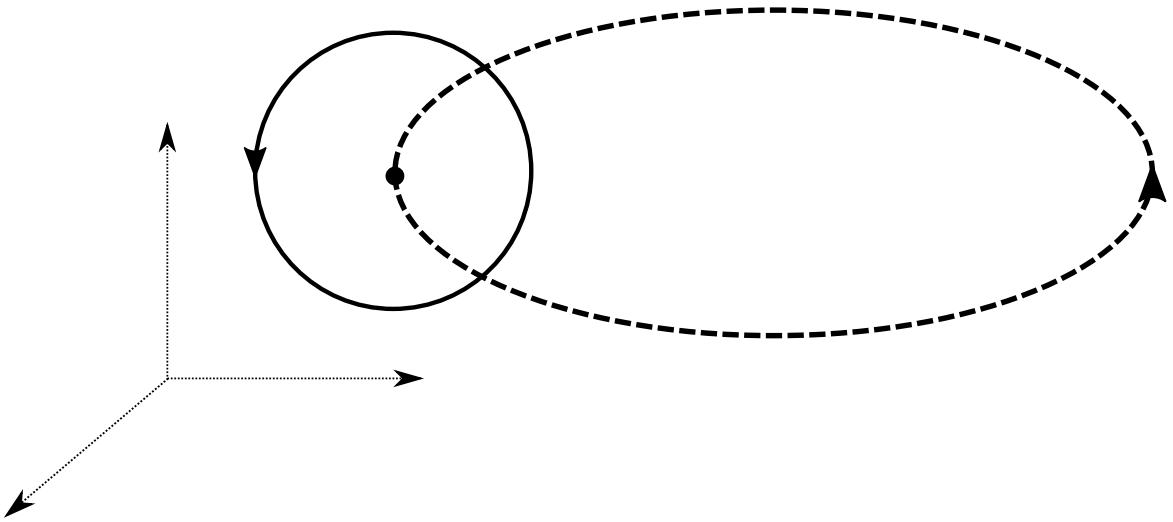

Fig. 3.1 A single centre vortex (dashed line) intersecting a Wilson loop (solid line) in 3 dimensions. The Wilson loop will acquire a centre phase corresponding to the phase of the vortex.

We can insert a complete set of energy eigenstates, $\sum_n |\, n\rangle \langle n\,| = 1$ to obtain

$$\begin{aligned} W(R \times T) &= \mathrm{Tr}\left(\sum_n \langle U_1(0)\,|\, n\rangle \langle n\,|\, e^{-E_n(R)\,T}\,|\, U_1(0)\rangle \right) \\ &= \sum_n \mathrm{Tr}\left(\left| \langle U_1(0)\,|\, n\rangle \right|^2 \right) e^{-E_n(R)\,T} \end{aligned}$$

As $T \to \infty$, the only surviving contribution will be the lowest energy, $E_0(R)$. This means that

$$\lim_{T\to\infty} W(R \times T) \propto e^{-E_0(R)\,T}\,. \tag{3.5}$$

With Eq. 3.5 in mind, we return to the aforementioned $SU(2)$ confinement model. Consider a two-dimensional plane with area L^2, with N vortices piercing the plane. Then the vortex density $\rho = \frac{N}{L^2}$. The probability of finding n vortex in some region of the plane A is equal to the probability that at least n vortices are in A, multiplied by the probability that at least $N-n$ vortices are outside of A. Expressed mathematically, this is

$$P_N(n) = \binom{N}{n} \left(\frac{A}{L^2}\right)^n \left(1 - \frac{A}{L^2}\right)^{N-n}\,. \tag{3.6}$$

In $SU(2)$ the group centre is simply $Z(2) = \pm I$, so the vortices each contribute a phase of -1. So the expectation value of the Wilson loop around the perimeter of A takes

the value

$$\langle W(\partial A)\rangle = \sum_{n=0}^{N}(-1)^n\, P_N(n) \tag{3.7}$$

$$= \left(1-\frac{A}{L^2}\right)^N \sum_{n=0}^{N}\binom{N}{n}\left(-\frac{A}{L^2}\left(1-\frac{A}{L^2}\right)^{-1}\right)^n \tag{3.8}$$

Making use of the binomial theorem to evaluate the sum in Eq. 3.8, we find

$$\langle W(\partial A)\rangle = \left(1-\frac{2A}{L^2}\right)^N . \tag{3.9}$$

We then re-express Eq. 3.9 in terms of the vortex density ρ

$$\langle W(\partial A)\rangle = \left(1-\frac{2\rho A}{N}\right)^N , \tag{3.10}$$

and take the limit as $L^2, N \to \infty$ whilst keeping ρ constant to obtain the final result

$$\lim_{N\to\infty}\langle W(\partial A)\rangle = \exp(-2\rho A)\,. \tag{3.11}$$

Taking $A = R \times T$, we see that from Eq. 3.5, Eq. 3.11 implies that $E_0 = 2\rho\, R$. Hence, the potential energy between two massive, static quarks increases linearly with the distance R separating them, which is precisely the confinement scenario!

It is important to highlight the assumptions and simplifications made in the above argument. Firstly, this

3.3 Locating Vortices

3.3.1 Maximal Centre Gauge

3.3.2 Centre Projection

3.4 Instantons

3.4.1 Topological Charge

Chapter 4

Landau Gauge Gluon Propagator

In a gauge field theory, the position-space propagator, $D_{\mu\nu}(x-y)$, of the gauge boson is the two-point correlation function, which in the case of $SU(3)$ can be interpreted as the probability of a gluon being created at position x, propagating to y, and then being annihilated. The propagator therefore serves as a useful measure of the behaviour of gluons as a function of distance; or, correspondingly, as a function of momentum in the momentum-space representation. In this chapter we detail how the Landau gauge gluon propagator is calculated on the lattice.

4.1 Lattice Definition of the Gluon Propagator

We begin with the definition of the coordinate space propagator [27, 40, 41].

$$D^{ab}_{\mu\nu}(x) = \langle A^a_\mu(x)\, A^b_\nu(0)\rangle. \tag{4.1}$$

The propagator in momentum space is simply related by the discrete Fourier transform,

$$D^{ab}_{\mu\nu}(p) = \sum_x e^{-ip\cdot x}\langle A^a_\mu(x)\, A^b_\nu(0)\rangle. \tag{4.2}$$

Noting that the coordinate space propagator $D^{ab}_{\mu\nu}(x-y)$ only depends on the difference $x-y$, such that

$$\langle A^a_\mu(x)\, A^b_\nu(0)\rangle = \langle A^a_\mu(x+y)\, A^b_\nu(y)\rangle\,, \tag{4.3}$$

we can make use of translational invariance to average over the four-dimensional volume to obtain the form for the momentum space propagator.

$$\begin{aligned} D^{ab}_{\mu\nu}(p) &= \frac{1}{V}\sum_{x,y} e^{-ip\cdot x}\langle A^a_\mu(x+y)\, A^b_\nu(y)\rangle \\ &= \frac{1}{V}\sum_{x,y}\langle e^{-ip\cdot(x+y)} A^a_\mu(x+y)\, e^{+ip\cdot y} A^b_\nu(y)\rangle \\ &= \frac{1}{V}\langle A^a_\mu(p)\, A^b_\nu(-p)\rangle. \end{aligned} \tag{4.4}$$

Hence we find that the momentum space gluon propagator on a finite lattice with four-dimensional volume V is given by

$$D^{ab}_{\mu\nu}(p) \equiv \frac{1}{V}\left\langle A^a_\mu(p)\, A^b_\nu(-p)\right\rangle . \tag{4.5}$$

In the continuum, the Landau-gauge momentum-space gluon propagator has the following form [7, 42]

$$D^{ab}_{\mu\nu}(q) = \left(\delta_{\mu\nu} - \frac{q_\mu q_\nu}{q^2}\right)\delta^{ab}\, D(q^2)\,, \tag{4.6}$$

where $D(q^2)$ is the scalar gluon propagator. Contracting Gell-Mann index b with a and Lorentz index ν with μ one has

$$D^{aa}_{\mu\mu}(q) = (4-1)\,(n_c^2-1)\, D(q^2)\,, \tag{4.7}$$

such that the scalar function can be obtained from the gluon propagator via

$$D(q^2) = \frac{1}{3(n_c^2-1)}\, D^{aa}_{\mu\mu}(q)\,, \tag{4.8}$$

where $n_c = 3$ is the number of colours.

As the lattice gauge links $U_\mu(x)$ naturally reside in the 3×3 fundamental representation of $SU(3)$, we now wish to work in the matrix representation of $A_\mu(x)$, as introduced in Eq. 2.3. Using the orthogonality relation $\mathrm{Tr}(\lambda_a\lambda_b) = \delta_{ab}$ for the Gell-Mann matrices, it is straightforward to see that

$$2\,\mathrm{Tr}(A_\mu\, A_\mu) = A^a_\mu A^a_\mu\,, \tag{4.9}$$

which can be substituted into equation 4.8 to obtain the final expression for the lattice scalar gluon propagator,

$$D(p^2) = \frac{2}{3\,(n_c^2 - 1)\,V}\Big\langle \mathrm{Tr}\, A_\mu(p)\, A_\mu(-p)\Big\rangle\,. \tag{4.10}$$

To calculate Eq. 4.10 on the lattice, we need to define $A_\mu(p)$. As defined in Eq. 2.21, we make use of the midpoint definition of the coordinate-space gauge potential in terms of the lattice link variables. Once the link variables are fixed to Landau gauge following the procedure described in Sec. 2.3.1, we obtain the momentum-space gauge potential

$$A_\mu(p) = \sum_x e^{-ip\cdot(x+\hat{\mu}/2)}\, A_\mu(x + \hat{\mu}/2)\,. \tag{4.11}$$

We have now constructed the necessary tools to calculate the Landau gauge scalar gluon propagator within the lattice framework established in Chapter 2.

4.2 Momentum Variables

As discussed in Sec. 3.1, it is understood that at QCD is asymptotically free. With this understanding, we expect that at high momentum the Landau gauge gluon propagator will tend towards the Landau gauge photon propagator [3]

$$D_\gamma(p^2) = \frac{1}{p^2}\,. \tag{4.12}$$

4.3 Lattice Parameters and Data Cuts

Chapter 5

Smoothing

Lattice definitions of topological objects are plagued by random fluctuations originating from the Monte-Carlo generation of lattice configuration and as a result they can often give inaccurate or nonsensical results. Hence, when considering the behaviour of topological objects on the lattice, it has been proven to be necessary to remove high frequency fluctuations in the gauge fields [43]. Furthermore, when investigating the long distance behaviour of the lattice it is also beneficial to filter off the short distance fluctuations to better reveal the physics in the region of interest [44]. For example, it has previously been shown that smoothing is necessary to obtain agreement between the untouched and vortex only string tension, mass function and instanton content [45–47]. The process of removing these fluctuations is known as smoothing, which in turn falls into two sub-categories: cooling and smearing.

The purpose of both these methods is similar, however, the algorithms used to implement them differ greatly. Cooling assesses each link, replacing the existing link with one that locally minimises some choice of action (see e.g. the Wilson action in Eq. 2.24). Smearing does not depend on the choice of action, and instead replaces each link with a weighted average of its nearest neighbours. Once every link in the lattice has been updated, the configuration is said to have had one sweep of smoothing applied. The process can then be repeated to an arbitrary number of sweeps. Due to the differences in the routines, it is important to compare the results from both to observe how they each perform and quantitatively observe how the alter the measured quantities.

5.1 Smoothing Methods

5.1.1 Cooling

Cooling is the original method devised for smoothing lattice gauge fields, first utilised in the analysis of the topological susceptibility of simplified lattice models [48]. It was shown early on that the process of cooling can be used to distinguish between 'genuine' topological charge representative of classical minima of the action, and background Monte-Carlo topological charge brought about by random fluctuations created during the generation of the lattice configuration. Under cooling, the former is preserved whilst the latter is annihilated. The process of cooling according to the simplest Wilson action is based on the method outlined by Cabibbo and Marinari [49, 50], and is performed as follows:

We first consider the Wilson action associated with a single link U_μ,

$$S(U_\mu) = 3 - \mathrm{Re}\,\mathrm{Tr}(U_\mu \bar{U})\,, \tag{5.1}$$

which is a different, but completely equivalent, form of Eq. 2.24. $\bar{U}$ is defined as the sum of the 'staples' associated with U_μ. A staple is defined as the product of all the link variables around a chosen loop, except for the link being cooled. For example, the 1×1 plaquette staple associated with U_μ is

$$\tilde{U}_\mu^{1\times 1}(x) = U_\nu(x+\hat{\mu})U_\mu^\dagger(x+\hat{\nu})U_\nu^\dagger(x)\,. \tag{5.2}$$

Graphically, this can be seen as in Fig. 5.1. Larger staples are defined similarly; for

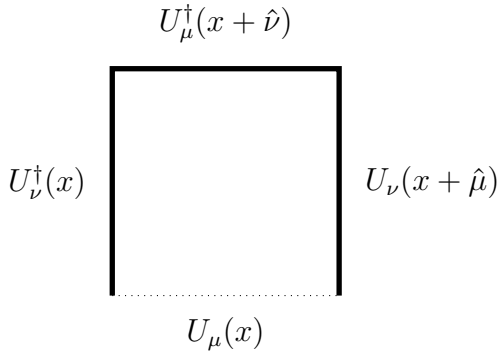

Fig. 5.1 An example 1×1 staple, with the dashed link indicating the link the staple is relative to. The origin of the name staple is apparent from the shape of the 3 solid links.

example a 2×2 staple corresponds to the product of seven of the eight links in the 2×2 square, with $U_\mu(x)$ omitted. For the Wilson action, the six unique 1×1 staples are the only ones required. Once all relevant staples are calculated, they are summed to obtain

$$\bar{U} = \sum_{\alpha=1}^{6} \tilde{U}_\alpha \,, \tag{5.3}$$

where α enumerates the staples, not the Lorentz index.

The objective of cooling is to select a new $SU(3)$ matrix to replace U_μ with some U'_μ that minimises Eq. 5.1, or equivalently, maximises

$$\mathrm{Re}\,\mathrm{Tr}(U'_\mu \bar{U}) \,. \tag{5.4}$$

Naively, it would seem that $U'_\mu = \bar{U}^{-1}$ would be the ideal choice. However, $\bar{U}$ is the sum of $SU(3)$ matrices, and $SU(3)$ is only closed under multiplication, not addition. Hence, $\bar{U}$, and by extension $\bar{U}^{-1}$, are not necessarily in $SU(3)$, making $\bar{U}^{-1}$ and invalid substitute for U_μ. However, any $SU(2)$ element can be written in the form $U = a_0 I + i\vec{a}\cdot\vec{\sigma}$, where $\vec{\sigma}$ are the Pauli matrices and $a \in \mathbb{R}$ satisfies $a^2 = 1$. Hence, a sum of $SU(2)$ elements is proportional to another $SU(2)$ element. We can exploit this fact to construct an new $SU(3)$ element from three $SU(2)$ subgroups. To this end, we wish to find a U' of the form

$$U'_\mu = a_3\, a_2\, a_1\, U_\mu \,, \tag{5.5}$$

where the a_i are each in different a 3×3 representation of $SU(2)$. We define the following three functions to take some $V \in SU(3) \to F_i(V) \in SU(2)$

$$F_1(V) = \frac{1}{k_1}\begin{pmatrix} \frac{1}{2}(V_{11}+V_{22}^*) & \frac{1}{2}(V_{12}-V_{21}^*) & 0 \\ \frac{1}{2}(V_{21}-V_{12}^*) & \frac{1}{2}(V_{11}^*+V_{22}) & 0 \\ 0 & 0 & 1 \end{pmatrix}$$

$$F_2(V) = \frac{1}{k_2}\begin{pmatrix} \frac{1}{2}(V_{22}+V_{33}^*) & 0 & \frac{1}{2}(V_{23}-V_{32}^*) \\ 0 & 1 & 0 \\ \frac{1}{2}(V_{32}-V_{23}^*) & 0 & \frac{1}{2}(V_{22}^*+V_{33}) \end{pmatrix}$$

$$F_3(V) = \frac{1}{k_3}\begin{pmatrix} 1 & 0 & 0 \\ 0 & \frac{1}{2}(V_{11}+V_{33}^*) & \frac{1}{2}(V_{13}-V_{31}^*) \\ 0 & \frac{1}{2}(V_{31}-V_{13}^*) & \frac{1}{2}(V_{11}^*+V_{33}) \end{pmatrix} \,,$$

where $k_i^2 = \det(k_i\, F_i(V))$ fixes the determinant such that $\det(F_i(V)) = 1$. We now wish to find a suitable V to define our a_i's. Consider the first case, $U_\mu^{(1)} = a_1\, U_\mu$, and let $a_1 = F_1(U_\mu\, \bar{U})^\dagger$. It is worth stating explicitly that it is this step where the fact that a sum of $SU(2)$ matrices is proportional to an $SU(2)$ matrix is utilised. Despite the fact that $U_\mu\, \bar{U} \notin SU(3)$, $U_\mu\, \tilde{U}_\alpha \in SU(3)$, which implies that $F_i(U_\mu\, \tilde{U}_\alpha) \in SU(2)$. Then we have

$$\sum_{\alpha=1}^{6} k_{i,\,\alpha}\, F_i(U_\mu\, \tilde{U}_\alpha) = k_i F_i(U_\mu \bar{U}) \tag{5.6}$$

$$\implies F_i(U_\mu \bar{U}) = \frac{1}{k_i} \sum_{\alpha=1}^{6} k_{i,\,\alpha}\, F_i(U_\mu\, \tilde{U}_\alpha) \in SU(2)\,,$$

where we have made use of the linearity of $k_i\, F_i$ to obtain Eq. 5.6. With this definition of a_1, the functional we are seeking to maximise evaluates to

$$\mathrm{Re}\,\mathrm{Tr}(F_1(U_\mu\, \bar{U})^\dagger\, U_\mu\, \bar{U}) = 2 + \mathrm{Re}(U_\mu\, \bar{U})_{33}\,. \tag{5.7}$$

The proof of this is given in Appendix A. By the matrix structure of $F_1(V)$ it is apparent that $\mathrm{Re}(U_\mu\, \bar{U})_{33}$ is invariant under pre-multiplication by a_1, so it is clear that Eq. 5.7 represents the maximum attainable value for this form of $U_\mu^{(1)}$. Similarly, we let $a_2 = F_2(U_\mu\, \bar{U})^\dagger$ and $a_3 = F_3(U_\mu\, \bar{U})^\dagger$ to obtain the final value of U'_μ according to Eq. 5.5. The above procedure is repeated over all three $SU(2)$ subgroups 12 times per lattice link to effectively minimise the local action. One sweep of cooling then constitutes applying this procedure to every link on the lattice.

As detailed in Ref. [43], this process can be thought of as locally minimising the Wilson action of the three $SU(2)$ subgroups, which collectively minimises the Wilson action of the full $SU(3)$ link. It is then simple to extend this procedure to different actions by expanding the size and shape of the staples considered in the construction of $\bar{U}$. As the only quantities utilised in the cooling procedure are gauge invariant, cooling can be performed in any gauge to arrive at the same cooled configuration. Cooling also maintains the Boltzmann distribution of the lattice links [49], indicating that the new links can be considered a thermalised distribution. However, cooling is not a gauge transformation, and as such it represents a deviation from the original physical configuration. We therefore need to be careful when selecting the action used for the cooling routine to ensure that we are not removing the physics that we are interested in. To best study instantons and topological charge on a periodic lattice, it

has been shown that a $\mathcal{O}(a^4)$ three-loop improved action is most suitable [51]. This choice of action combines both computational efficiency with an effective stabilisation of instantons and an accurate preservation of the topological charge under repeated cooling sweeps. This action is dubbed a 'three-loop' action as it consists of a linear combination of 1×1, 2×2 and 3×3 Wilson loops.

5.1.2 Over-Improved Smearing

Despite the accurate results obtained from cooled lattice configurations, cooling presents certain computational inefficiencies. Given that the staples, $\bar{U}_\alpha$ must remain constant while updating a given link U_μ, there are limitations to how parallelised the algorithm can be, especially for larger combinations of loops such as those used in the chosen three-loop improved action. To avoid these issues, a different type of smoothing was developed, known as 'smearing'. Rather than locally minimising the action by direct substitution of each link, the initial APE smearing [52, 53] routine replaces each link with a weighted average of its nearest neighbours, according to

$$U' = (1 - \alpha)\, U_\mu + \frac{\alpha}{6}\, \bar{U}^\dagger \,, \tag{5.8}$$

where $\bar{U}$ is the sum of the staples given in Eq. 5.3 and α is some weighting parameter. However, as stated in the previous section, a linear combination of $SU(3)$ matrices is not necessarily in $SU(3)$, so APE smearing is dependent on a choice of projection into the $SU(3)$ group. To remove the need for this projection step, the method of stout-link smearing was developed [54].

Much like in the case of cooling, it is easiest to begin by considering smearing in terms of the Wilson action, then extending this to the over-improved case utilised in this research. To begin, we define

$$\Sigma_\mu = \rho_{\text{sm}}\, (U_\mu\, \bar{U})^\dagger \,, \tag{5.9}$$

where ρ_{sm} is a smearing constant chosen to remain fixed for all lattice sites. Using this definition we construct

$$Q_\mu = \frac{i}{2}\left(\Sigma_\mu^\dagger - \Sigma_\mu\right) - \frac{i}{6}\,\text{Tr}\left(\Sigma_\mu^\dagger - \Sigma_\mu\right) I \,. \tag{5.10}$$

By construction Q_μ is Hermitian ($Q_\mu = Q_\mu^\dagger$) and traceless, so it belongs to the $SU(3)$ Lie algebra. It can therefore be exponentiated to obtain an element of $SU(3)$. We then define the new smeared link by

$$U'_\mu = \exp(iQ_\mu)\, U_\mu \,. \tag{5.11}$$

This definition effectively corresponds to a complex sum of neighbouring link combinations, however it has numerically been demonstrated to give similar results to the previous APE smearing technique, provided that the smearing parameter ρ is selected appropriately [54]. As in the case of cooling, the choice of staples used to define $\bar{U}$ has significant impact on the behaviour of topological objects under smearing. To this end, work has been done to tune the smearing algorithm so that it preserves instanton-like objects under repeated smearing sweeps, leading to the development of over-improved stoutlink smearing [44].

To quantitatively measure the effect of smearing on topological objects, it is common to calculate the instanton action in terms of the instanton radius. The error terms in the instanton action then give an indication of how the instanton radius will change as the action decreases under smearing.

5.2 Results from the Gluon Propagator

Making use of the smoothing methods defined above, we now wish to compare their effect on the gluon propagator. We first plot the untouched propagator after 0, 1, 2, 4 and 8 sweeps of cooling in Fig. 5.2. In gauge fixing to Landau gauge, each sweep has been preconditioned by the Landau gauge transformation of the prior sweep in descending order (i.e. the transformation for sweep 10 preconditions sweep 9). This preconditioning is done to ensure that the Landau gauge functional is near the same local minima for each cooling sweep. We observe the expected removal of short distance fluctuations that is typical of smoothing, resulting in a suppressed propagator at large q. This is complemented by an amplification in the infra-red region which can be attributed to the increase in low momentum modes arising from the smoothing of the gauge fields.

To compare the effects of cooling and over-improved smearing, the untouched gluon propagator is plotted in Fig. 5.3 after either over-improved smearing or cooling. By

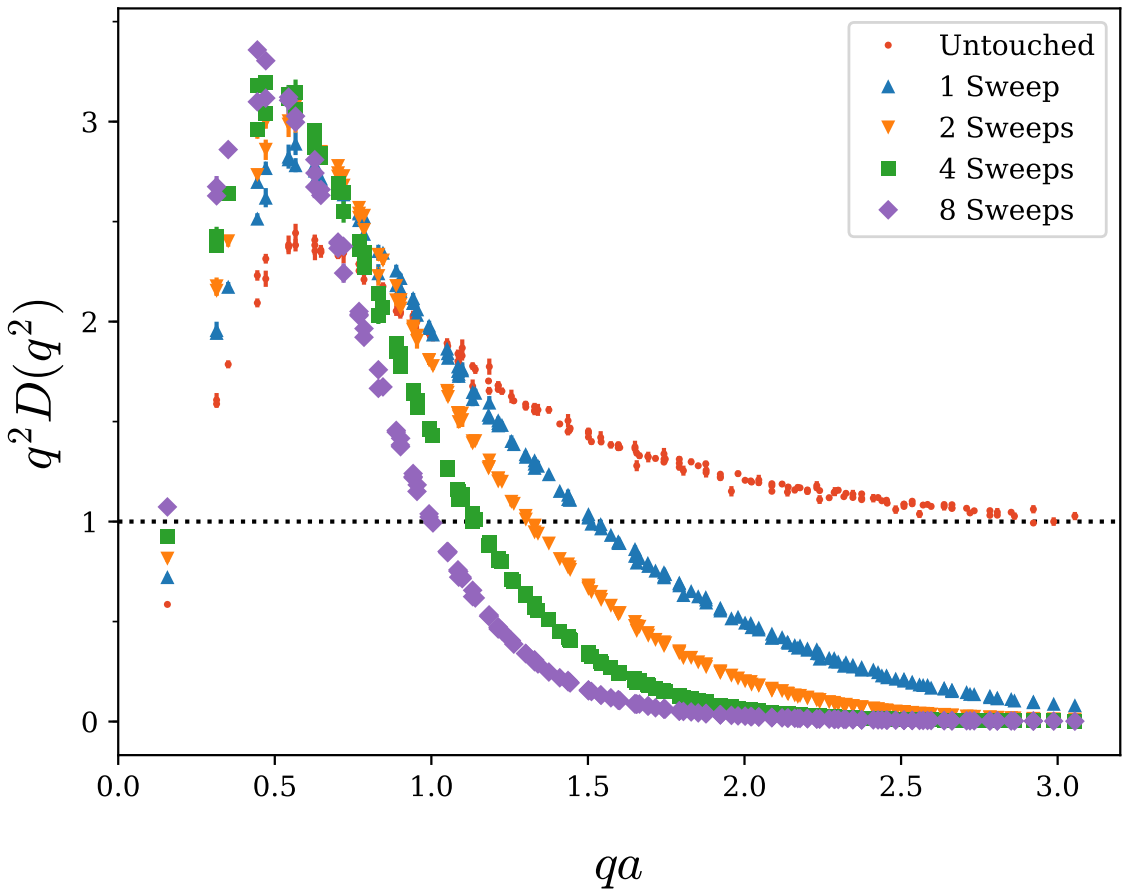

Fig. 5.2 Comparison of the gluon propagator on the untouched configurations after cooling. For clarity we have selected a sample of sweeps between 1 and 8.

comparing the smeared and cooled propagator we can see that cooling has a more rapid effect, related to the well-known fast removal of action from the lattice. The qualitative shape of the propagator remains the same however, and it can be seen that, for example, 4 smearing sweeps produces a propagator remarkably similar to 1 cooling sweep. More generally, we observe that in regards to the shape of the propagator, $n_{\text{sm}} \approx 4\, n_{\text{cool}}$. Following the observation made in Ref. [55] that the number of over-improved stoutlink smearing sweeps is related to the gradient flow time by

$$t \approx \rho\, n_{\text{sm}}\,, \tag{5.12}$$

we deduce that the relationship between gradient flow time and cooling is

$$t \approx 0.24\, n_{\text{cool}}\,. \tag{5.13}$$

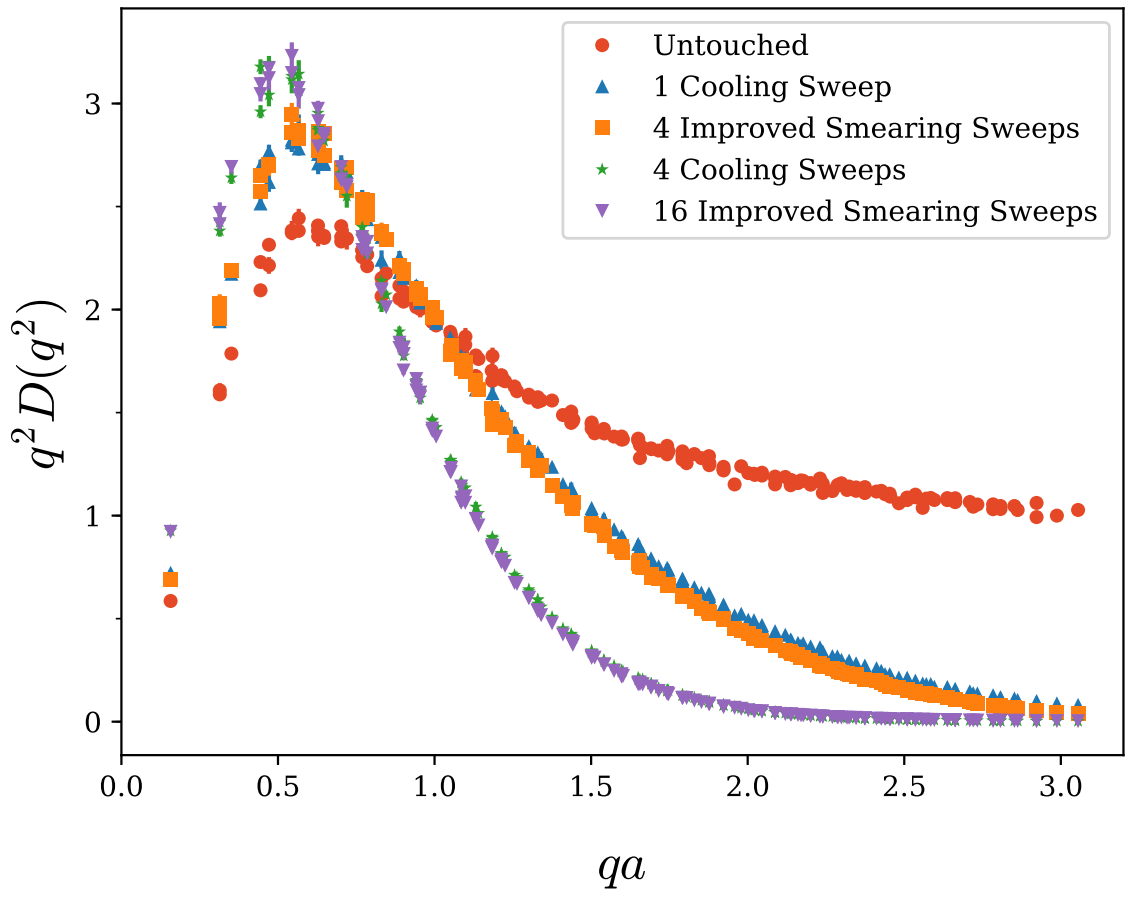

Fig. 5.3 The gluon propagator after cooling or improved smearing. We see that the shape of the plot changes minimally between the smoothing routines. However cooling requires fewer sweeps to produce the same effect when compared to smearing.

It is well understood that smoothing alters the vortex background, and based on previous work [45, 56, 57] we anticipate that the vortices identified on smoothed configurations would differ to those identified on the unsmoothed configurations. We therefore perform vortex identification only on the original configurations, with smoothing then being performed independently on the untouched, vortex-only and vortex-removed configurations. We choose to use cooling as the smoothing algorithm for the results presented in this paper, however it is worth noting that similar results can be obtained with the use of over-improved smearing.

Chapter 6

Gluon Propagator on Vortex-Modified Backgrounds

Here we present the results from the gluon propagator, calculated according to method outlined in Chapter 4, on our three vortex-modified configurations:

1. Original 'untouched' fields, $U_\mu(x)$,
2. Projected vortex-only fields, $Z_\mu(x)$,
3. Vortex-removed fields, $R_\mu(x) = Z_\mu^\dagger(x)\, U_\mu(x)$.

6.1 Preliminary Results

Calculating the scalar propagator on untouched, vortex-removed and vortex only configurations gives the results illustrated in Fig. 6.1. To make contact with the tree-level propagator at large q^2, we renormalise such that $q^2 D(q^2) = 1$ for $qa = 3.0$ on the original configurations, and apply this same renormalisation factor to the vortex removed and vortex only propagators. The vortex removed configurations display the expected behaviour, with vortex removal corresponding to significant infrared suppression of the propagator when compared to the untouched propagator, in agreement with the results of Ref. [58]. The increased roughness of the gauge fields after vortex removal is evidenced by the enhancement of the propagator at large q. This reflects the increase in short-distance fluctuations that have been introduced to the gauge fields by the vortex removal procedure.

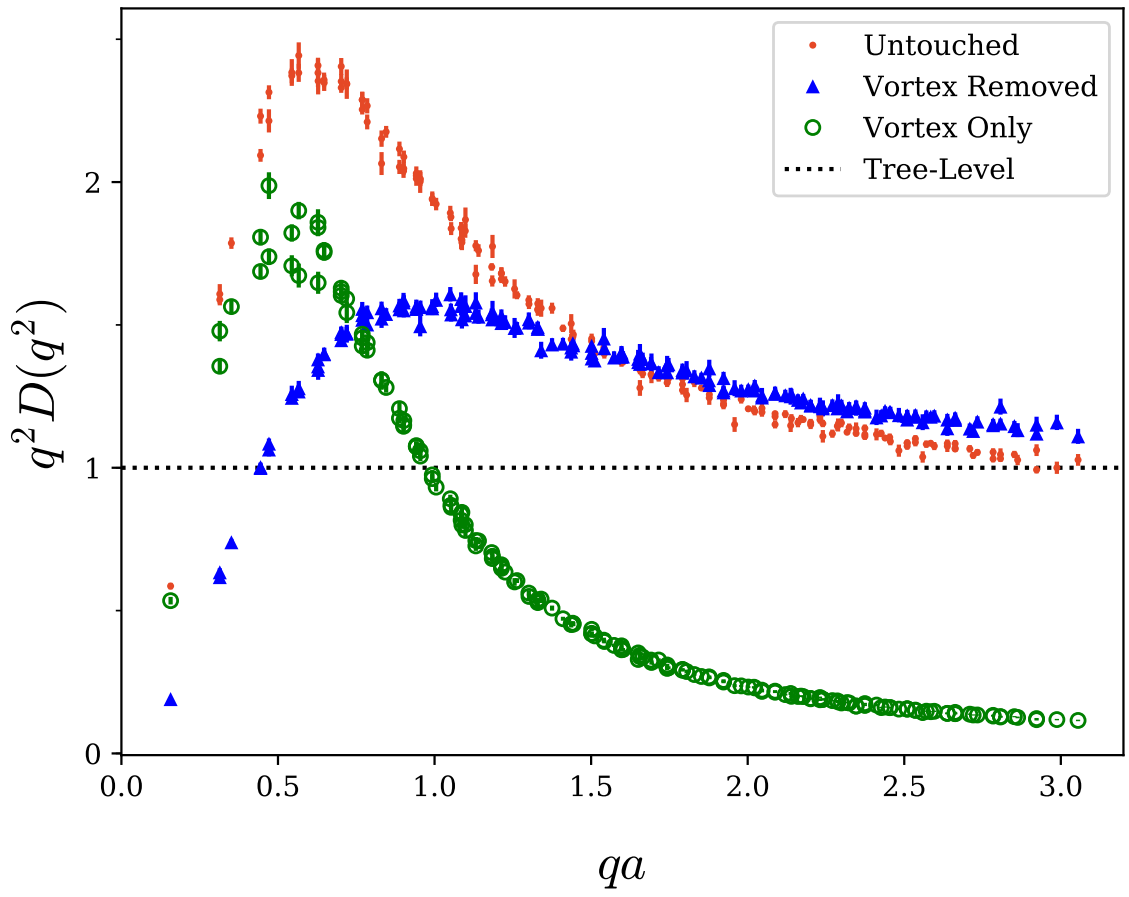

Fig. 6.1 The gluon propagator calculated from the original untouched (red dots), shown with the vortex removed (blue triangles) and vortex only (green open circles) results. Here, the renormalisation factor for the vortex removed and vortex only propagators is chosen to be the same as for the untouched propagator.

It is interesting to note that the vortex only propagator retains approximately two thirds of the untouched propagator's peak strength. This is comparable to previous work showing partial recovery of the string tension on vortex only configurations [45, 47, 59, 60]. Despite only recovering a portion of the original strength, the infrared peak is still considerably greater than the peak observed in the vortex removed propagator. The loss of strength is most likely in part because of the known imperfections in the vortex identification algorithm that results in some vortex matter remaining in the vortex removed configurations. The vortex only configurations also exhibit a loss of short range strength, due to the absence of the high frequency modes that are instead contained within the vortex removed field.

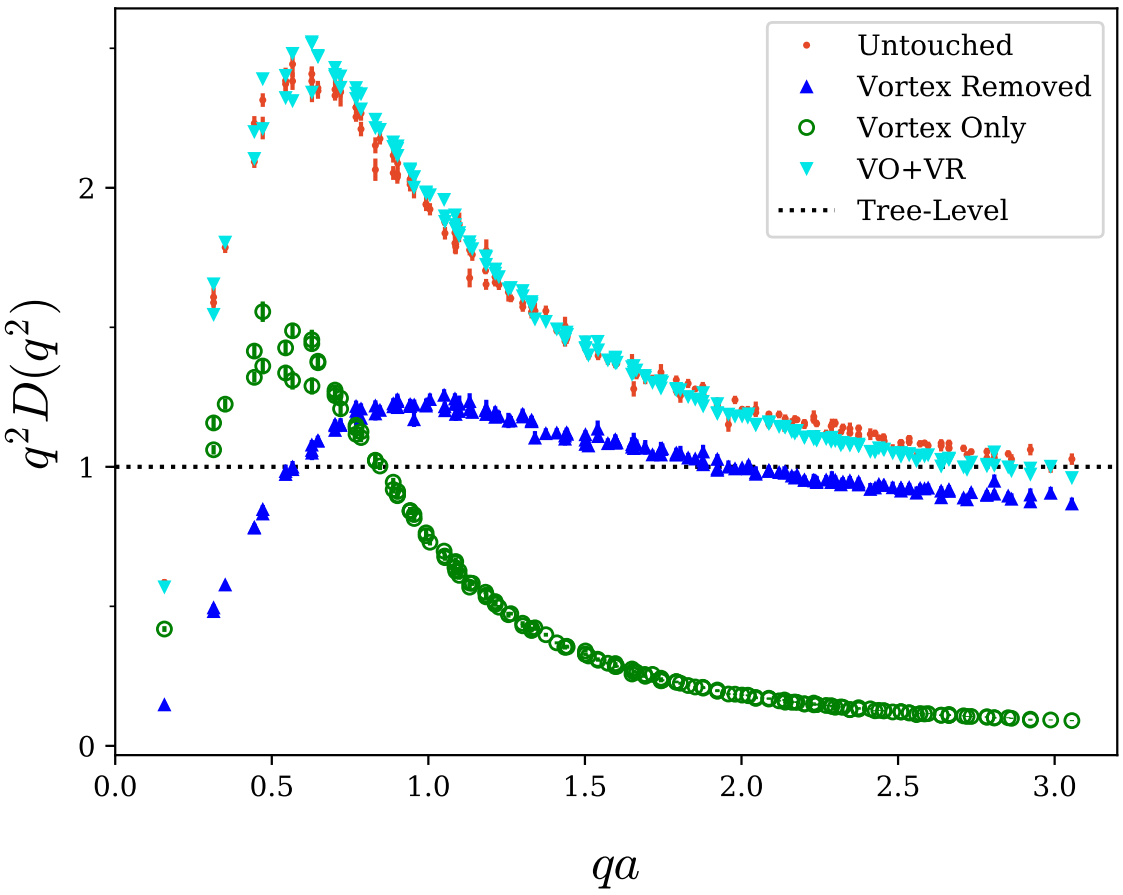

Fig. 6.2 The gluon propagator from the original untouched ensemble as in Fig. 6.1, now shown with the independently renormalised sum (cyan triangles) of the vortex removed and vortex only propagators. The two vortex modified propagators are also shown, but here their renormalisation factor is chosen to be the same as for the summed propagator.

If we sum the vortex only and vortex removed propagators and independently renormalise such that $q^2\,D(q^2) = 1$ at $qa = 3.0$, we obtain the result shown in Fig. 6.2. Here we observe agreement between the untouched and summed propagators. This indicates that vortex modification effectively partitions the lattice configuration into short range physics on the vortex removed configurations and long range physics on the vortex only configurations, up to errors in the vortex identification procedure.

6.1.1 Partitioning

This partitioning is expected if the vortex removed and vortex only configurations are orthogonal. To see how this behaviour emerges, suppose that we can decompose the

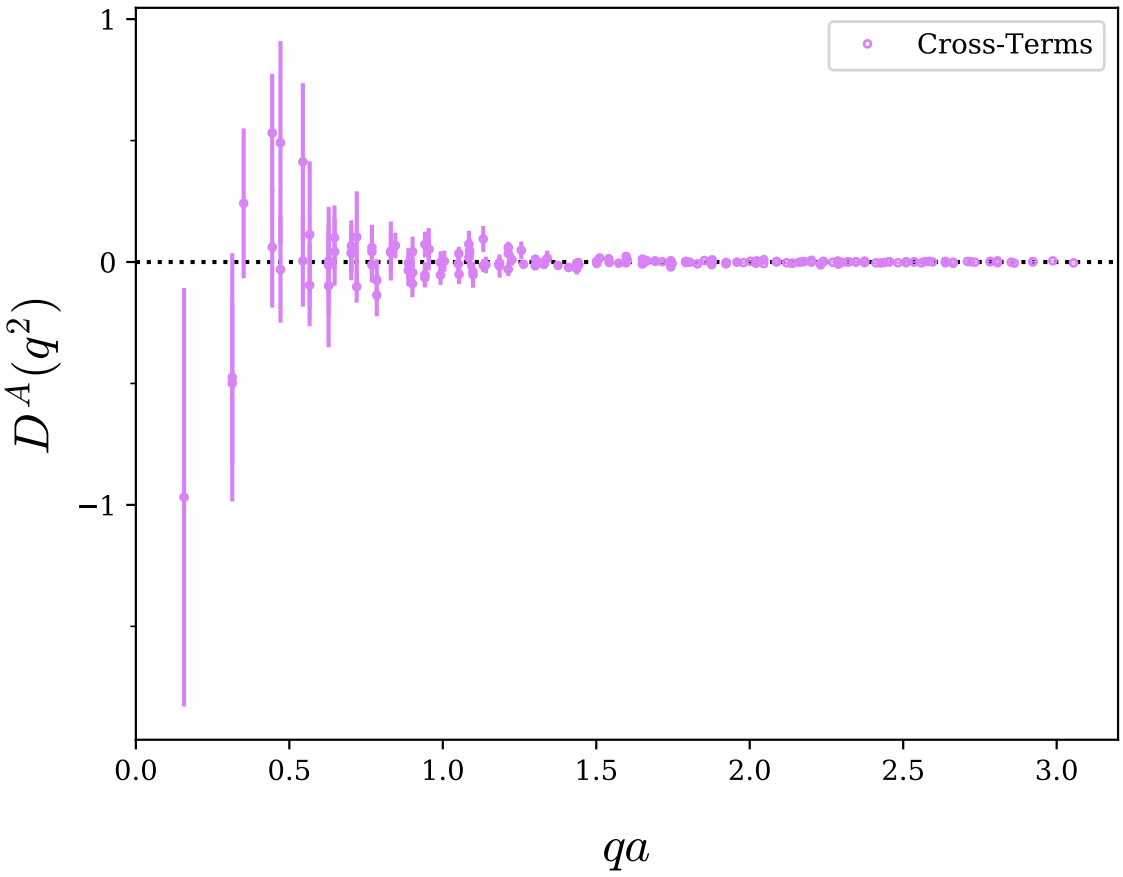

Fig. 6.3 Calculation of the cross-terms arising from Eq. 6.2

gluon field A_μ into two independent fields as follows

$$A_\mu(p) = B_\mu(p) + C_\mu(p). \tag{6.1}$$

In the context of this work, we associate B_μ with the background field of short-range gluon fluctuations and C_μ with the centre vortex field. Note also that if B and C are in Landau gauge then so is A. Using this partitioning it follows that the gluon propagator

for A can be written as the sum of the respective gluon propagators for B and C,

$$\begin{aligned} D^A_{\mu\nu}(p) &= \frac{1}{V}\langle A_\mu(p)\, A_\nu(-p)\rangle \\ &= \frac{1}{V}\Big(\langle B_\mu(p)B_\nu(-p)\rangle + \langle C_\mu(p)C_\nu(-p)\rangle \\ &\qquad + \langle B_\mu(p)C_\nu(-p) + C_\mu(p)B_\nu(-p)\rangle\Big) \\ &= D^B_{\mu\nu}(p) + D^C_{\mu\nu}(p), \end{aligned} \tag{6.2}$$

where we have made use of the fact that B and C represent orthogonal degrees of freedom in the gauge field and hence in the ensemble average the cross-correlations should vanish. These cross-correlations are explicitly calculated by evaluating

$$D_{\text{cross-terms}}(p^2) = \frac{2}{3\,(n_c^2-1)\,V}\,\langle \mathrm{Tr}\,(B_\mu(p)C_\mu(-p) + C_\mu(p)B_\mu(-p))\rangle\ , \tag{6.3}$$

analogous to the scalar gluon propagator derived in Chapter 4. The results of this calculation are shown in Fig. 6.3. As can be clearly seen, in the ensemble average Eq. 6.3 vanishes, indicating that the vortex only and vortex removed configurations truly do represent a orthogonal degrees of freedom.

To elucidate the connection to the unitary formulation of the lattice gauge links, we suppose that we can transform A to an "ideal centre gauge" such that in lattice units the field C consists purely of centre phases,

$$C_\mu(x) = k\,\frac{2\pi}{3}I, \quad k \in \{-1, 0, +1\}. \tag{6.4}$$

On a continuous manifold we can write the Wilson line corresponding to a lattice link as a path-ordered exponential,

$$U_\mu(x) = \mathcal{P}e^{i\int_0^1 d\lambda\, A_\mu(x+\lambda\hat{\mu})}. \tag{6.5}$$

The lattice midpoint approximation replaces the integral as follows,

$$U_\mu(x) = e^{iA_\mu(x+\hat{\mu}/2)}. \tag{6.6}$$

As $A = B + C$ it immediately follows that we can write

$$U_\mu(x) = e^{iB_\mu(x+\hat{\mu}/2)}\, e^{iC_\mu(x+\hat{\mu}/2)}, \tag{6.7}$$

noting that in our ideal centre gauge $[B, C] = 0$ so the Baker-Campbell-Haussdorff relation is trivial. Identifying

$$Z_\mu(x) = e^{iC_\mu(x+\hat{\mu}/2)} \tag{6.8}$$

as the vortex-projected field, and

$$R_\mu(x) = e^{iB_\mu(x+\hat{\mu}/2)} \tag{6.9}$$

as the background remainder field we thus recover the decomposition of the links used herein,

$$U_\mu(x) = Z_\mu(x) \cdot R_\mu(x). \tag{6.10}$$

In practise, on the lattice the maximal centre gauge fixing that is implemented will differ from the ideal centre gauge postulated here due to apparent numerical difficulties in simultaneously identifying all vortex matter within an $SU(3)$ gauge field. What this means is that the projected field Z may not capture all of the vortex matter such that there is some non-trivial topological structures that remain in the background field R. The infrared enhancement in the vortex removed results in Fig. 6.1 suggests this is the case.

6.1.2 Renormalisation

In Fig. 6.2 it proved necessary to independently renormalise the untouched and summed propagators such that they agree at $qa = 3.0$. The necessity of this renormalisation is worth discussing, as it is important to motivate why comparison between the original and reconstructed propagators is valid.

Renormalisation steps:

1. Calculation contains divergent integrals that must be isolated.
2. Dimensional regularisation isolates the infinities in the integral.
3. Redefine the mass/coupling to absorb these infinities. The new constant is *finite*, whereas the original constant is taken to be *infinite*.
4. Alternatively, the counter term method can be used.
5. The counter term method states that the original constant is *finite*, that are modified by infinite constants.

6. Upon calculating physical quantities, the infinite constants cancel off the infinities arising from the loop integrals.

Questions:

1. At what scale does $D_{\mathrm{QED}}(q^2) = \frac{1}{q^2}$?
2. At what scale can we suppose that $D_{\mathrm{QED}}(q^2) = D_{\mathrm{QCD}}(q^2)$
3. Is it reasonable to say that the condition that must be enforced on the combined propagator is $D(q^2) = \frac{1}{q^2}$ at some large momentum, and as such this is the normalisation that should be applied to the VR and VO propagators?
4. Does $D_{\mathrm{QCD}}(q^2)$ equal the bare continuum propagator at a fixed cutoff?
5. What does the renormalised propagator correspond to in the continuum?

6.2 Impact of Cooling

After performing 10 sweeps of cooling on the untouched, vortex-removed and vortex-only ensembles, we obtain the results shown in Fig. 6.4. As is typical of cooling, the removal of short range structures means that all three ensembles tend to zero as $q \to \infty$. There is now a noticeable improvement in the agreement between the untouched and vortex only configurations; however there is still a difference present, especially in the $qa \approx 0.5$ and $qa \approx 1.5$ regions.

We perform the same analysis of the vortex only propagator under cooling as performed in Sec. 5.2 on the untouched propagator. Once again in gauge fixing, each sweep is preconditioned by the Landau gauge transformation of the previous sweep in descending order. The result of this analysis is shown in Fig. 6.5. This figure shows a similar change in the vortex only propagator when compared to the untouched propagator in Fig. 5.2, with an enhancement in the infrared and suppression in the UV modes. The UV suppression is less noticeable in this case due to the prior removal of short range effects brought about by the vortex identification.

We observe that the vortex only and untouched propagators in Fig. 6.4 resemble the gluon propagator under a differing number of sweeps of cooling, as shown in Fig. 5.2 and Fig. 6.5. The vortex only propagator has a peak that sits below the untouched

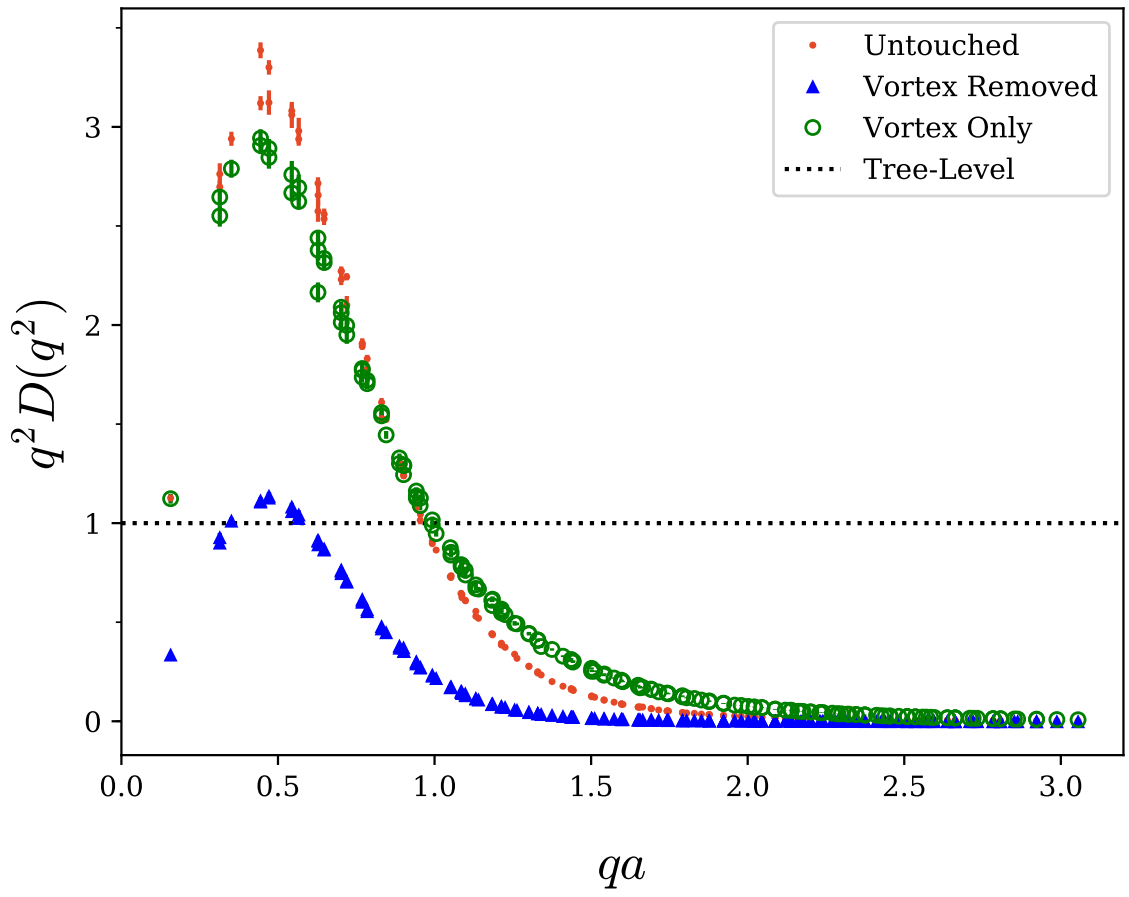

Fig. 6.4 The gluon propagator calculated on the three ensembles after 10 sweeps of cooling. We now observe an improved agreement between the untouched and vortex only propagators.

propagator, and the untouched propagator is further suppressed in the $qa \approx 1.5$ region. Following the trend in Fig. 5.2 and Fig. 6.5, this indicates that further cooling on the vortex only propagator would align it with the untouched propagator. This follows from an understanding that the vortex-only configurations are initially much rougher than their untouched counterparts [46], and should therefore require additional cooling to obtain agreement with the untouched configurations.

We take the average $\mathcal{O}(a^4)$ three-loop improved action of the lattice divided by the single instanton action $S_0 = \frac{8\pi^2}{g^2}$, denoted $\bar{S}/S_0$, to be a measure of roughness. We observe that for $n < 20$ cooling sweeps the vortex-only configurations have a significantly higher action than their untouched counterparts after the same number of sweeps of cooling, as illustrated in Fig. 6.6. We therefore seek to find the number

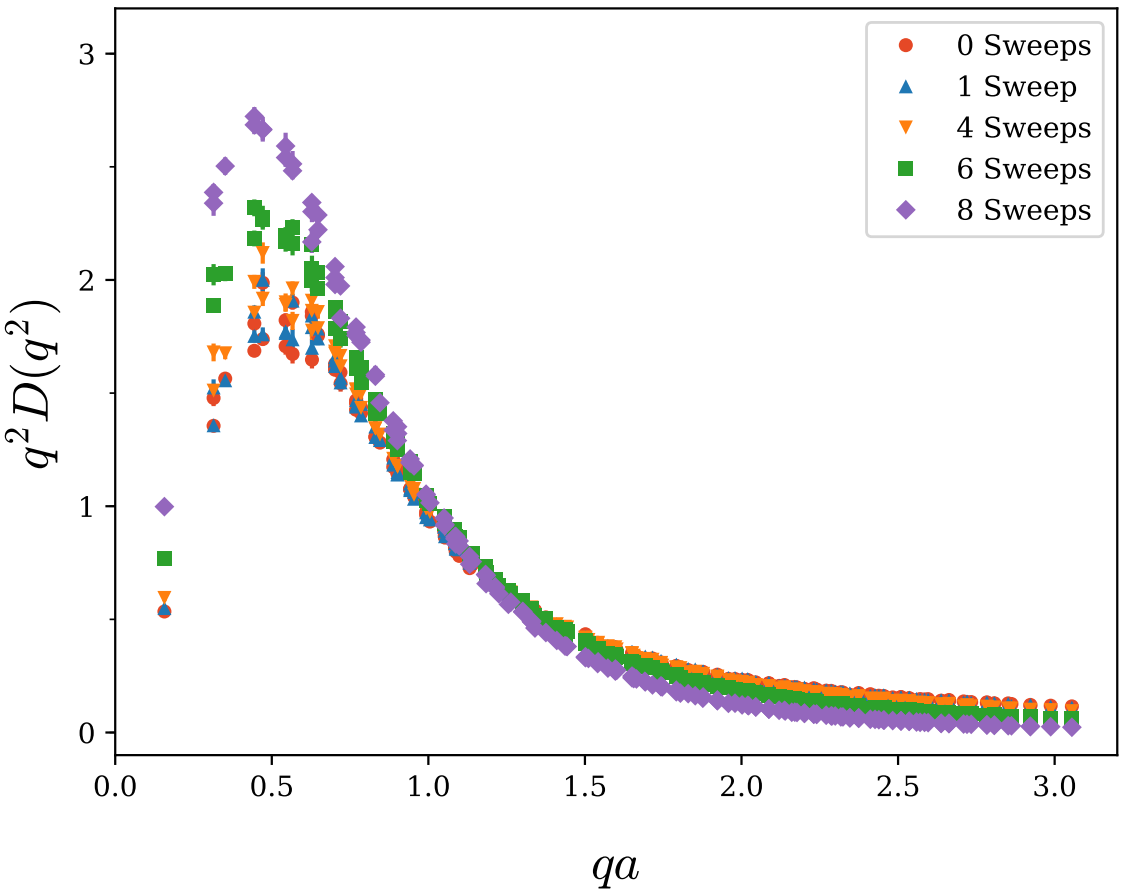

Fig. 6.5 The vortex only propagator after different sweeps of cooling. A trend similar to Fig. 5.2 is observed, with enhancement in the infrared and suppression in the UV region.

of sweeps required to best match the action between the vortex-only and untouched configurations. The results of this procedure are shown in Table 6.1. If we now plot these matched configurations, we obtain the results shown in Fig. 6.7. Here we have truncated the plot at large qa to better show the agreement in the mid-qa region. By matching the actions as closely as possible with an integer number of cooling sweeps, we see that there is a better agreement between the untouched and vortex-only gluon propagators.

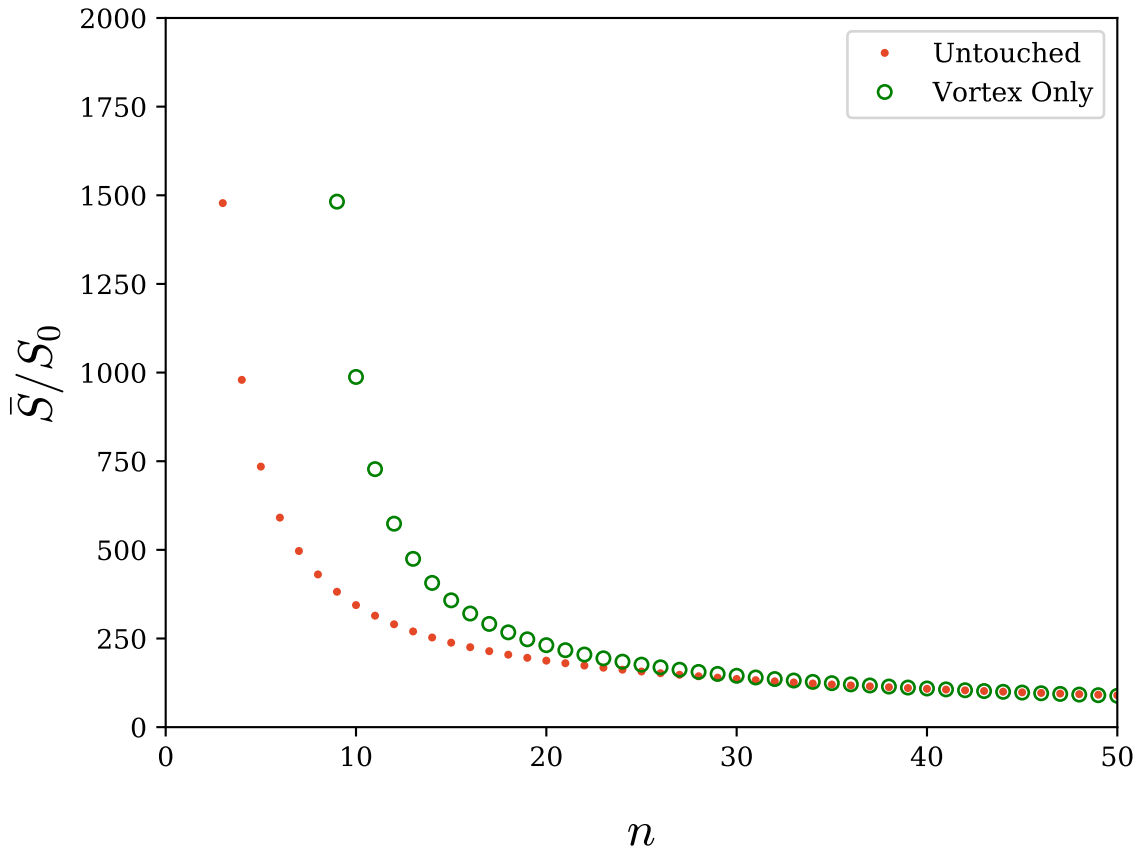

Fig. 6.6 The average action calculated on the untouched and vortex-only configurations as a function of cooling sweeps, n. The vortex only configurations are initially rougher than the untouched, as evidenced by the higher average action.

Table 6.1 Comparison of the number of cooling sweeps on the untouched (n_U) and vortex only (n_{VO}) configurations required to match the average action.

n_U	$\bar{S}/S_0$	n_{VO}	$\bar{S}/S_0$
5	734.83	11	727.67
10	344.22	15	357.68
15	238.21	20	231.19
20	187.55	24	184.68
25	156.92	28	155.72
30	135.91	32	135.61
35	120.29	36	120.66
40	107.08	40	109.02

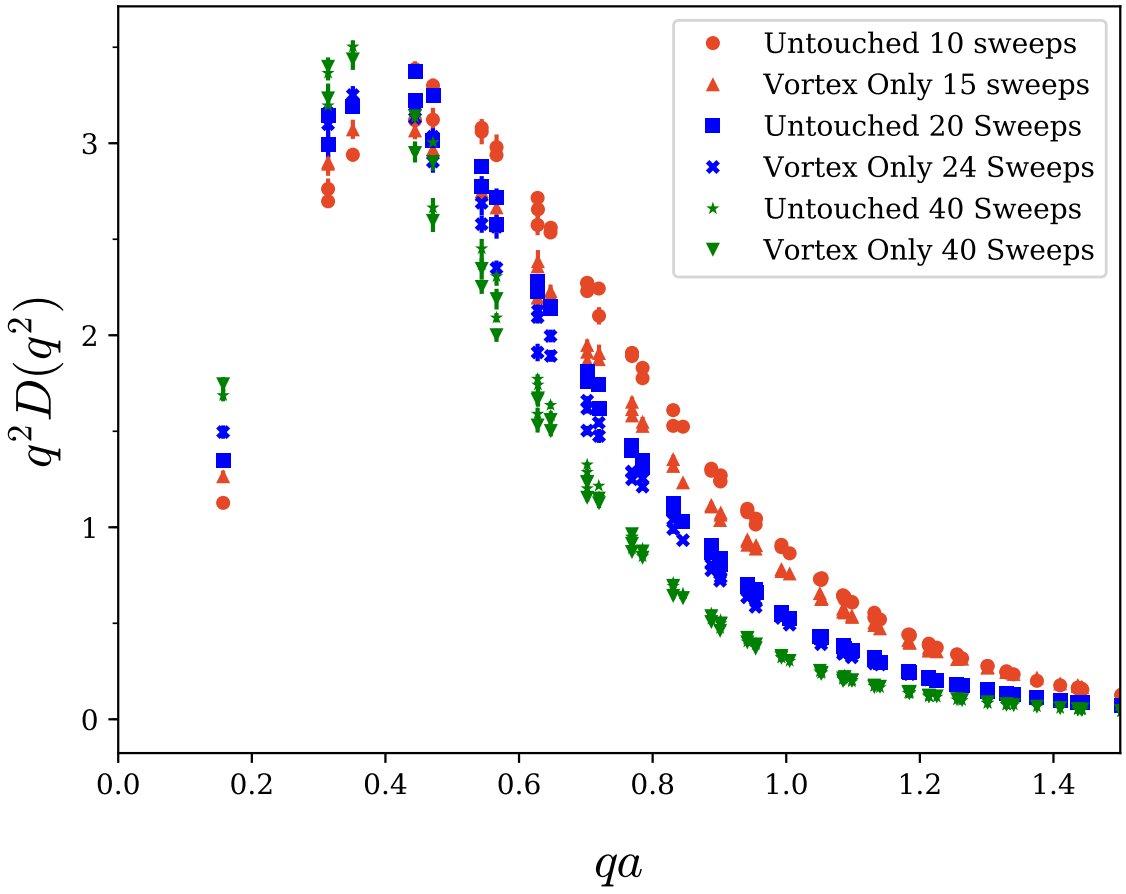

Fig. 6.7 Comparison of the gluon propagator on the untouched and vortex only configurations after tuning the number of cooling sweeps to best match the average plaquette action. This procedure gives a much better agreement in the shape of the gluon propagator from the two configurations.

Chapter 7

Centre Vortex Visualisations

7.1 3D Models

7.1.1 Time Slices

7.1.2 Time-Oriented Links

7.1.3 Topological Charge

7.2 Centre Vortices and Topological Charge

Chapter 8

Conclusion

References

[1] Kenneth G. Wilson. Confinement of Quarks. *Phys. Rev.*, D10:2445–2459, 1974. [,319(1974)].

[2] Michael E Peskin. *An introduction to quantum field theory*. CRC Press, 2018.

[3] Lewis H Ryder. *Quantum field theory*. Cambridge university press, 1996.

[4] Thomas Schäfer and Edward V. Shuryak. Instantons in QCD. *Rev. Mod. Phys.*, 70:323–426, 1998.

[5] Hurl Bing and Lin He. Gauge symmetry from integral viewpoint. 1999.

[6] G. P. Lepage. Lattice QCD for novices. In *Strong interactions at low and intermediate energies. Proceedings, 13th Annual Hampton University Graduate Studies, HUGS'98, Newport News, USA, May 26-June 12, 1998*, pages 49–90, 1998.

[7] Derek B. Leinweber, Jon Ivar Skullerud, Anthony G. Williams, and Claudio Parrinello. Gluon propagator in the infrared region. *Phys. Rev.*, D58:031501, 1998.

[8] B. Alles, D. Henty, H. Panagopoulos, C. Parrinello, C. Pittori, and D. G. Richards. α_s from the nonperturbatively renormalised lattice three gluon vertex. *Nucl. Phys.*, B502:325–342, 1997.

[9] Rajan Gupta. Introduction to lattice QCD: Course. In *Probing the standard model of particle interactions. Proceedings, Summer School in Theoretical Physics, NATO Advanced Study Institute, 68th session, Les Houches, France, July 28-September 5, 1997. Pt. 1, 2*, pages 83–219, 1997.

[10] Mark G. Alford, W. Dimm, G. P. Lepage, G. Hockney, and P. B. Mackenzie. Lattice QCD on small computers. *Phys. Lett.*, B361:87–94, 1995.

[11] K. Symanzik. Continuum Limit and Improved Action in Lattice Theories. 1. Principles and phi**4 Theory. *Nucl. Phys.*, B226:187–204, 1983.

[12] K. Symanzik. Continuum Limit and Improved Action in Lattice Theories. 2. O(N) Nonlinear Sigma Model in Perturbation Theory. *Nucl. Phys.*, B226:205–227, 1983.

[13] M. Luscher and P. Weisz. On-Shell Improved Lattice Gauge Theories. *Commun. Math. Phys.*, 97:59, 1985. [Erratum: Commun. Math. Phys.98,433(1985)].

[14] G. Peter Lepage and Paul B. Mackenzie. On the viability of lattice perturbation theory. *Phys. Rev.*, D48:2250–2264, 1993.

[15] Frederic D. R. Bonnet, Patrick O. Bowman, Derek B. Leinweber, Anthony G. Williams, and David G. Richards. Discretization errors in Landau gauge on the lattice. *Austral. J. Phys.*, 52:939–948, 1999.

[16] Murray Gell-Mann. A Schematic Model of Baryons and Mesons. *Phys. Lett.*, 8:214–215, 1964.

[17] G. Zweig. An SU(3) model for strong interaction symmetry and its breaking. Version 2. In D.B. Lichtenberg and Simon Peter Rosen, editors, *DEVELOPMENTS IN THE QUARK THEORY OF HADRONS. VOL. 1. 1964 - 1978*, pages 22–101. 1964.

[18] Robert Hofstadter. Electron scattering and nuclear structure. *Rev. Mod. Phys.*, 28:214–254, 1956.

[19] Elliott D. Bloom et al. High-Energy Inelastic e p Scattering at 6-Degrees and 10-Degrees. *Phys. Rev. Lett.*, 23:930–934, 1969.

[20] Martin Breidenbach, Jerome I. Friedman, Henry W. Kendall, Elliott D. Bloom, D. H. Coward, H. C. DeStaebler, J. Drees, Luke W. Mo, and Richard E. Taylor. Observed Behavior of Highly Inelastic electron-Proton Scattering. *Phys. Rev. Lett.*, 23:935–939, 1969.

[21] Richard P. Feynman. Very high-energy collisions of hadrons. *Phys. Rev. Lett.*, 23:1415–1417, 1969. [,494(1969)].

[22] David J. Gross and Frank Wilczek. Ultraviolet Behavior of Nonabelian Gauge Theories. *Phys. Rev. Lett.*, 30:1343–1346, 1973. [,271(1973)].

[23] K. D. Born, E. Laermann, R. Sommer, P. M. Zerwas, and T. F. Walsh. The Interquark potential: A QCD lattice analysis. *Phys. Lett.*, B329:325–331, 1994.

[24] Frederic D. R. Bonnet, Derek B. Leinweber, Anthony G. Williams, and James M. Zanotti. Towards string breaking in the static quark potential. *Submitted to: Phys. Rev. D*, 1999.

[25] Michael Creutz. Monte Carlo Study of Renormalization in Lattice Gauge Theory. *Phys. Rev.*, D23:1815, 1981.

[26] Adriano Di Giacomo, Michele Maggiore, and Stefan Olejnik. Confinement and Chromoelectric Flux Tubes in Lattice QCD. *Nucl. Phys.*, B347:441–460, 1990.

[27] D. Zwanziger. Vanishing of zero momentum lattice gluon propagator and color confinement. *Nucl. Phys.*, B364:127–161, 1991.

[28] Y. Iwasaki, K. Kanaya, S. Sakai, and T. Yoshie. Quark confinement and number of flavors in strong coupling lattice QCD. *Phys. Rev. Lett.*, 69:21–24, 1992.

[29] A. A. Belavin, Alexander M. Polyakov, A. S. Schwartz, and Yu. S. Tyupkin. Pseudoparticle Solutions of the Yang-Mills Equations. *Phys. Lett.*, B59:85–87, 1975. [,350(1975)].

[30] Gerard 't Hooft. How Instantons Solve the U(1) Problem. *Phys. Rept.*, 142:357–387, 1986.

[31] T. L. Ivanenko, A. V. Pochinsky, and M. I. Polikarpov. Extended Abelian monopoles and confinement in the SU(2) lattice gauge theory. *Phys. Lett.*, B252:631–635, 1990.

[32] M. N. Chernodub and F. V. Gubarev. Instantons and monopoles in maximal Abelian projection of SU(2) gluodynamics. *JETP Lett.*, 62:100–104, 1995.

[33] Curtis G. Callan, Jr., Roger F. Dashen, and David J. Gross. A Mechanism for Quark Confinement. *Phys. Lett.*, 66B:375–381, 1977.

[34] S. Mandelstam. Vortices and Quark Confinement in Nonabelian Gauge Theories. *Phys. Rept.*, 23:245–249, 1976.

[35] Gerard 't Hooft. The Topological Mechanism for Permanent Quark Confinement in a Nonabelian Gauge Theory. *Phys. Scripta*, 25:133–142, 1982.

[36] Gerard 't Hooft. On the Phase Transition Towards Permanent Quark Confinement. *Nucl.Phys.*, B138:1, 1978.

[37] Gerard 't Hooft. A Property of Electric and Magnetic Flux in Nonabelian Gauge Theories. *Nucl.Phys.*, B153:141, 1979.

[38] Jeff Greensite. Confinement from Center Vortices: A review of old and new results. *EPJ Web Conf.*, 137:01009, 2017.

[39] Yuri Makeenko. A Brief Introduction to Wilson Loops and Large N. *Phys. Atom. Nucl.*, 73:878–894, 2010.

[40] Attilio Cucchieri. Infrared behavior of the gluon propagator in lattice Landau gauge: The Three-dimensional case. *Phys. Rev.*, D60:034508, 1999.

[41] K. Langfeld, H. Reinhardt, and J. Gattnar. Gluon propagators and quark confinement. *Nucl. Phys.*, B621:131–156, 2002.

[42] Frederic D. R. Bonnet, Patrick O. Bowman, Derek B. Leinweber, Anthony G. Williams, and James M. Zanotti. Infinite volume and continuum limits of the Landau gauge gluon propagator. *Phys. Rev.*, D64:034501, 2001.

[43] Frederic D. R. Bonnet, Patrick Fitzhenry, Derek B. Leinweber, Mark R. Stanford, and Anthony G. Williams. Calibration of smearing and cooling algorithms in SU(3): Color gauge theory. *Phys. Rev.*, D62:094509, 2000.

[44] Peter J. Moran and Derek B. Leinweber. Over-improved stout-link smearing. *Phys. Rev.*, D77:094501, 2008.

[45] Daniel Trewartha, Waseem Kamleh, and Derek Leinweber. Connection between center vortices and instantons through gauge-field smoothing. *Phys. Rev.*, D92(7):074507, 2015.

[46] Daniel Trewartha, Waseem Kamleh, and Derek Leinweber. Evidence that centre vortices underpin dynamical chiral symmetry breaking in SU(3) gauge theory. *Phys. Lett.*, B747:373–377, 2015.

[47] Daniel Trewartha, Waseem Kamleh, and Derek Leinweber. Centre vortex removal restores chiral symmetry. *J. Phys.*, G44(12):125002, 2017.

[48] B. Berg. Dislocations and Topological Background in the Lattice O(3) σ Model. *Phys. Lett.*, 104B:475–480, 1981.

[49] N. Cabibbo and E. Marinari. A New Method for Updating SU(N) Matrices in Computer Simulations of Gauge Theories. *Phys. Lett.*, 119B:387–390, 1982.

[50] M. Creutz. Monte Carlo Study of Quantized SU(2) Gauge Theory. *Phys. Rev.*, D21:2308–2315, 1980.

[51] Sundance O. Bilson-Thompson, Derek B. Leinweber, and Anthony G. Williams. Highly improved lattice field strength tensor. *Annals Phys.*, 304:1–21, 2003.

[52] M. Albanese et al. Glueball Masses and String Tension in Lattice QCD. *Phys. Lett.*, B192:163–169, 1987.

[53] M. Falcioni, M. L. Paciello, G. Parisi, and B. Taglienti. AGAIN ON SU(3) GLUEBALL MASS. *Nucl. Phys.*, B251:624–632, 1985.

[54] Colin Morningstar and Mike J. Peardon. Analytic smearing of SU(3) link variables in lattice QCD. *Phys. Rev.*, D69:054501, 2004.

[55] Samuel D. Thomas, Waseem Kamleh, and Derek B. Leinweber. Instanton contributions to the low-lying hadron mass spectrum. *Phys. Rev.*, D92(9):094515, 2015.

[56] Alan O'Cais, Waseem Kamleh, Kurt Langfeld, Ben Lasscock, Derek Leinweber, Peter Moran, Andre Sternbeck, and Lorenz von Smekal. Preconditioning Maximal Center Gauge with Stout Link Smearing in SU(3). *Phys. Rev.*, D82:114512, 2010.

[57] L. Del Debbio, Manfried Faber, J. Giedt, J. Greensite, and S. Olejnik. Detection of center vortices in the lattice Yang-Mills vacuum. *Phys. Rev.*, D58:094501, 1998.

[58] Patrick O. Bowman, Kurt Langfeld, Derek B. Leinweber, Andre Sternbeck, Lorenz von Smekal, and Anthony G. Williams. Role of center vortices in chiral symmetry breaking in SU(3) gauge theory. *Phys. Rev.*, D84:034501, 2011.

[59] Kurt Langfeld. Vortex structures in pure SU(3) lattice gauge theory. *Phys. Rev.*, D69:014503, 2004.

[60] John D. Stack, W. W. Tucker, and Roy J. Wensley. The Maximal Abelian gauge, monopoles, and vortices in SU(3) lattice gauge theory. *Nucl. Phys.*, B639:203–222, 2002.

Appendix A

Evaluation of $\mathrm{Re}\,\mathrm{Tr}(F_1(U)^\dagger\, U)$

It is apparent that we can write Eq. 5.7 in the form

$$\mathrm{Re}\,\mathrm{Tr}(F_1(U)^\dagger\, U)\,, \tag{A.1}$$

where $U = U_\mu\,\bar{U}$. Expanding this, we have

$$\begin{aligned}\mathrm{Re}\,\mathrm{Tr}(F_1(U)^\dagger\, U) &= \mathrm{Re}\left(\frac{1}{2}\,U_{11}\,(U_{22}+U_{11}^*) - \frac{1}{2}\,U_{21}\,(U_{12}-U_{21}^*)\right.\\ &\quad\left.+\,\frac{1}{2}\,U_{22}\,(U_{11}+U_{22}^*) - \frac{1}{2}\,U_{12}\,(U_{21}-U_{12}^*) + U_{33}\right)\\ &= \mathrm{Re}\left(\frac{|U_{11}|^2}{2}+\frac{|U_{22}|^2}{2}+\frac{|U_{12}|^2}{2}+\frac{|U_{21}|^2}{2}+U_{11}\,U_{22}-U_{12}\,U_{21}+U_{33}\right)\,.\end{aligned}$$

We now wish to make use of the known determinant of $F_1(U)$ to simplify this expression.

$$\begin{aligned}\det(F_1(U)) &= \frac{1}{4}\,(U_{11}+U_{22}^*)\,(U_{11}^*+U_{22})\\ &\quad-\frac{1}{4}\,(U_{12}-U_{21}^*)\,(U_{21}-U_{12}^*)\\ &= \frac{1}{4}\left(|U_{11}|^2+|U_{22}|^2+|U_{12}|^2+|U_{21}|^2\right.\\ &\quad\left.+\,U_{11}\,U_{22}+U_{11}^*\,U_{22}^*+U_{12}\,U_{21}+U_{12}^*\,U_{21}^*\right)=1\,,\end{aligned}$$

and hence

$$\mathrm{Re}(\det(F_1(U))) = \frac{1}{2}\,\mathrm{Re}\left(\frac{|U_{11}|^2}{2}+\frac{|U_{22}|^2}{2}+\frac{|U_{12}|^2}{2}+\frac{|U_{21}|^2}{2}+U_{11}\,U_{22}-U_{12}\,U_{21}\right)=1\,. \tag{A.2}$$

So we find the desired result

$$\mathrm{Re}\,\mathrm{Tr}(F_1(U)^\dagger U) = 2 + \mathrm{Re}(U_{33}) \tag{A.3}$$